

Constrained Decision-making for Low-count Radiation Detection by Mobile Sensors

Jianxin Sun and Herbert G. Tanner

Received: date / Accepted: date

Abstract This paper approaches from an optimal control perspective the problem of fixed-time detection of mobile radioactive sources in transit by means of a collection of mobile sensors. Under simplifying assumptions on the motion and geometry of the source, the sensors, and the surrounding environment, the optimal control problem admits an intuitive, analytic closed-form solution. This solution is obtained thanks to analytic expressions for bounds on the probabilities of detection and false alarm for a Neyman-Pearson detection test. The intuition derived from this analytic solution supports the development of a motion control law that steers (suboptimally) the sensors to a given neighborhood of the suspected source, while navigating among stationary obstacles in their environment. This motion controller closes the loop at the acceleration level of a heterogeneous collection of sensor platforms. Experimental studies with these platforms corroborate the theoretical convergence results.

1 Introduction

This paper derives analytic optimal motion strategies for mobile sensors aiming at detecting weak radioactive sources in transit. It then investigates provably convergent relaxations which afford hardware implementation in constrained environments under constraints on actuation. The risk associated with this detection problem is encoded in two types of errors that can be made in the

decision-making process: a false alarm in which the system erroneously classifies a target as radioactive, and a missed detection where the system fails to recognize a radioactive source. In the context of nuclear detection, one tries to minimize the probability of missing a source under an upper bound (usually very small, for practical reasons) on the acceptable probability of false alarm.

Detecting radioactive sources is relevant and timely due to the increasing risk of accidental or malicious nuclear material proliferation (Archibold and Gladstone, 2013; Broad, 2012) and the need for inspecting vehicles and humans safely and without hindering traffic flow. To detect radioactive sources in transit from a distance, one solution (Byrd et al, 2005) is the deployment of a large network of spatially distributed detectors. Fast and remote radiation detection requires sophisticated equipment which does not come cheap (Byrd et al, 2005); yet one inexpensive, possibly miniaturized, radiation detector appropriate for such deployment is the Geiger counter.

Geiger counters merely record radiation rays hitting their internal crystal, regardless if these rays come from the source to be detected or from naturally occurring background radiation. The question thus is whether the aggregate count is due to background alone or to the superposition of background and source. This problem can be formulated as a binary hypothesis test—when there is a deadline, this becomes a fixed-time interval test—that has received considerable coverage in the literature (Brémaud, 1981). When detecting radioactive material, the perceived rate of count reception at each sensor changes with the distance between the sensor and the source, giving rise to a dynamic, time-inhomogeneous stochastic process. As a result, analytic characterization for the error probabilities in this decision problem is not possible. Yet, analytic expressions

Work supported in part by ARL MAST CTA # W911NF-08-2-0004.

Jianxin Sun E-mail: jxsun@udel.edu · Herbert G. Tanner E-mail: btanner@udel.edu
Department of Mechanical Engineering, University of Delaware

are central to designing motion control strategies for the mobile sensors that optimize detection probability.

For the most part, approaches in available literature attempt to identify not only the nature of the target but also its location solely based on radiation counters (Brennan et al, 2005; Chin et al, 2010; Nemzek et al, 2004). Such approaches essentially face a combination of problems—detection and localization—which is inherently very challenging, both at an analytical and computational level. For static sensors and source, a location estimator can be constructed, and a sequential probability ratio test can be formed (Chin et al, 2010). In addition to estimating the source’s position, algorithms within a Bayesian framework can also estimate source intensity (Brennan et al, 2005; Nemzek et al, 2004). Reported results support the hypothesis that sensor networks can be effective in remotely detecting static radiation sources. When the source is in motion, however, the associated analytic complexity translates to significantly increased computational complexity, and updating posterior probabilities using Bayes rule becomes problematic, even for networks of modest size (Nemzek et al, 2004) and under assumptions on the motion of the source being linear and with constant acceleration.

In contrast, this paper focuses on one of the constituent problems—namely, detection. We try to identify what is the best that can be done, under the *assumption* that the emission characteristics and trajectory of the source are known. The rationale behind this divide-and-conquer strategy is that on one hand, given the security application in mind, one probably has an idea of the type of material that is expected to be found. On the other hand, a multitude of other sensing modalities (e.g. cameras (Wei et al, 2014)) can be used to detect and track a mobile target; one does not need to track motion based solely on Geiger counters.

Although the separation between radiation detection and localization allows for an analytical optimal solution to the problem of mobile sensors deployment, eventually this solution has to be realized on physical systems under an array of real-world limitations and constraints. One of those constraints is related to environmental obstructions, or obstacles. To enable our mobile sensors to negotiate these obstacles while adhering to the spirit of the optimal deployment strategy, we adopt a feedback-based motion planning approach that utilizes a particular type of artificial potential functions known as navigation functions. The existing navigation function approach, however, cannot be directly applied to the problem at hand, because the destination is a time-varying set. The (arguably limited) existing work (Ghaffarkhah and Mostofi, 2009; Goncalves et al, 2010)

on time-varying potential fields does not cover the case considered here completely, in the sense that there can be *both* static obstacles *and* a time-varying target set, and in addition convergence—rather than merely ultimate boundedness—is required. We thus introduce new extensions and offer theoretical guarantees of algorithmic completeness and correctness.

The particular motion planning problem considered here is an instance of a general *time-varying* problem of navigating amongst obstacles. When it is the environment that is time-varying, e.g., the obstacles are moving, the problem has been approached from the perspective of roadmaps (Ziegler and Stiller, 2009). Optimal trajectories can be generated based on these roadmaps; however, as the dimensionality of the problem—primarily due to multiple platforms—increases, computational complexity presents some serious challenges. Alternatives that promise to preserve optimality (at least asymptotically) at a smaller computational cost, include PRM* and RRT* (Karaman and Frazzoli, 2011). These algorithms have been adapted to various situations that require fast generation of new solutions amongst obstacles (Choudhury et al, 2013; Marble and Bekris, 2013; Perez et al, 2012). Although asymptotically optimal in theory, appropriate extension heuristics have to be carefully chosen. At the end, there is always a trade-off between real-time performance and optimality.

Dealing with dynamic environments in real-time presents computational challenges to any sampling based technique. For this reason, this paper adopts a potential (navigation) function approach. Although a sampling-based planner may offer optimal paths—which a potential field controller cannot guarantee—on-line trajectory adaptation imposes stringent constraints on the computational power mobile platforms should carry.

The time-varying nature of the workspace presents unique challenges to potential function based controllers too. Existing work has treated instances of moving obstacles, particularly in cases where the “obstacles” are simultaneously deployed sensor platforms (Dimarogonas et al, 2006; Loizou et al, 2003; Tanner and Boddu, 2012). When moving entities are all controllable, this problem reduces to an instance of a (bigger) time invariant one. Avoiding collisions with both static and moving objects within a navigation function framework, however, needs to be treated with extreme care, because one of the basic working assumptions of the original methodology of Koditschek and Rimon (1990) no longer holds: obstacles can no longer guaranteed to be some ϵ apart. This issue is not addressed here; instead, the novelty of the navigation function approach used in this paper is in its ability to handle moving destinations with provable convergence guarantees.

2 Approach overview

In our two-stage approach (Fig 1), a high-level layer identifies the strategy that the mobile sensors have to follow to maximize their probability of detecting their targets, and a lower-level layer implements those strategies within the constraints imposed by sensor platform dynamics, actuation constraints, observation limitations, and environmental interactions.

In the upper layer, the optimal motion strategy for a mobile sensor is found analytically in the context of Maximum Principle. We will see that this results in a type of bang-bang solution, the intuitive interpretation of which is that sensors are managed optimally if they are brought as close to the source, as quickly as possible. Such a bang-bang control strategy would ignore sensor platform dynamics, would require unbounded accelerations, and introduce large transients.

A new (navigation function) potential field is then employed at the lower level to implement this strategy, taking now into consideration environment constraints (obstacles) and target motion. The outcome of this motion planner is a time-dependent velocity reference, which is then translated into reference inputs tailored to the dynamics of a particular platform — this is where robot dynamics are being incorporated. It is at this stage where actuator commands are being prescribed and subsequently realized. With the implementation of these commands, sensors collect observations that also inform about the state of the platforms in relation to their environment and their target. This information allows the potential field motion planner to update its velocity references, and close the control loop at the lower layer of the architecture.

In this framework the only part that needs to be changed when the sensor network changes size is the motion planning part. The optimal strategy is independent of the number of sensors that needs to be used.

3 Background: Networked Radiation Detection

Imagine that there is a mobile target which could be carrying a radioactive (point) source of activity a . The trajectory of this target is denoted $x_t(t) \in \mathbb{R}^3$. We assume that $\|\dot{x}_t\| \leq V_t$ for $t \in [0, T]$. In the specific setting considered in this paper, the target is to be classified as benign or radioactive within a time period of T seconds using a collection of k_s mobile sensors (radiation counters). The motion of the radiation sensors is controllable, and the trajectory of sensor i for $i \in \{1, \dots, k_s\}$ is denoted $x_i(t) \in \mathbb{R}^3$. The source activity a is measured in gamma rays emitted per second (cps). In this way, the source activity has the same units as sensor i 's

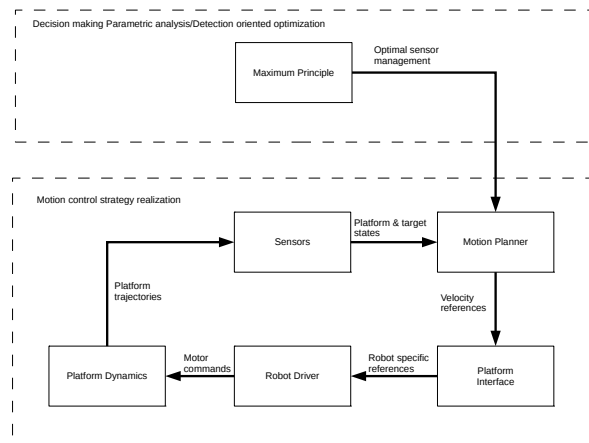


Fig. 1 Control & decision making architecture

cumulative observations up to time $t \in [0, T]$, denoted $N_t(i)$. For a fixed t and i , $N_t(i)$ is a random variable following a Poisson distribution. Each ray incident on sensor i is an event and the instant that the n th such event occurs at sensor i is denoted $\tau_n(i)$.

Such cumulative observations N_t are due not only to the alleged radioactive source, but also due to ubiquitous, naturally occurring, background radiation. In this paper, we assume that the source intensity is comparable to background. The background radiation intensity at the location of sensor i is denoted b_i and will be considered constant. Sensors cannot differentiate between counts due to source and counts due to background. Although background intensity can be assumed constant over limited space and time interval, the *perceived* source intensity by sensor i changes with the distance between the source and sensor i . Specifically, the closer the sensor is to the source, the more gamma rays from the source it is likely to register. If sensor i is assumed to have cross section coefficient χ_i for $i \in \{1, \dots, k_s\}$, then it is generally accepted [Nemzek et al (2004)] that the mean count rate ν_i measured by sensor i would follow an inverse square law with respect to the distance between sensor and source. We take this inverse square relationship to be of the form¹

$$\nu_i \triangleq \frac{\chi_i a}{2\chi_i + \|x_i - x_t\|^2} . \quad (1)$$

If a single sensor were to make a decision at time T as to whether the target it is observing is radioactive, it would have to choose between two hypotheses:

\mathcal{H}_0 : the target is not radioactive and the mean of the Poisson process which $N_T(i)$ follows is b_i , or

¹ When $\|x_i - x_t\| = 0$, the source is touching the surface of the sensor, and the latter measures exactly half of source's emitted rays.

\mathcal{H}_1 : the target is radioactive, and the mean of the Poisson process which $N_T(i)$ follows is $b_i + \nu_i$.

The decision is assumed to be made by a single processor—possibly one of the sensors—which collects the information and performs a likelihood ratio test (Pahlajani et al, 2014a). This processor is called the fusion center.

To analyze this decision problem we need the appropriate mathematical setting. For a given i , we recognize $N_t(i)$ as a Poisson process, and we collect all of these processes in a k -dimensional Poisson process $\mathbf{N}_t = (N_t(i), \dots, N_t(k_s))$ —the bold notation marks vectors formed by stacking vectors or scalars from all sensors. If we consider the set of all possible outcomes, that is, occurrences of such events on all sensors, we form a set Ω . Then we consider a measurable space (Ω, \mathcal{F}) , where \mathcal{F} is a σ -algebra on Ω .

Now let $(\mathcal{F}_t^{\mathbf{N}} : 0 \leq t \leq T)$ be the filtration generated by \mathbf{N}_t . This $\mathcal{F}_T^{\mathbf{N}}$ represents the collective information obtained from all sensors up to time T . Then the decision between hypothesis \mathcal{H}_0 and \mathcal{H}_1 on the basis of $\mathcal{F}_T^{\mathbf{N}}$ is equivalent to choosing the correct measure on $(\Omega, \mathcal{F}_T^{\mathbf{N}})$. For example, the choice of the probability measure \mathbb{P}_0 yields a probability space $(\Omega, \mathcal{F}_T^{\mathbf{N}}, \mathbb{P}_0)$ consistent with hypothesis \mathcal{H}_0 ; similarly, \mathbb{P}_1 with \mathcal{H}_1 . A particular valuation of \mathbf{N}_T is assumed to be an outcome $\omega \in \Omega$, and a test for deciding \mathcal{H}_1 takes the form of choosing a set $A_1 \in \mathcal{F}_T^{\mathbf{N}}$ and checking whether $\omega \in A_1$. A “false alarm” occurs when we find $\omega \in A_1$ while \mathcal{H}_0 is in force. The probability for making such an error is therefore $\mathbb{P}_0(A_1)$. Similarly, missing the radioactive target happens when $\omega \in (\Omega \setminus A_1)$ when \mathcal{H}_1 is in force, and the probability for such an error is $\mathbb{P}_1(\Omega \setminus A_1)$.

If $\tau_n(i)$ denotes the time instance at which sensor i recorded its n count, and $N_T(i)$ is the total number of counts registered by sensor i up to final time T , a Neyman-Pearson likelihood ratio test for the presence of a source can be of the form (Pahlajani et al, 2014a)

$$\prod_{i=1}^{k_s} \exp\left(-\int_0^T \nu_i(s) ds\right) \prod_{n=1}^{N_T(i)} \left(1 + \frac{\nu_i(\tau_n(i))}{b_i(\tau_n(i))}\right) \geq \gamma \quad (2)$$

and methods are known (Pahlajani et al, 2014b) for the analytical selection of threshold γ based on target and sensor trajectories. An optimal motion coordination strategy for the sensors could be one that maximizes the probability detection $\mathbb{P}_1(A_1)$ under an upper bound constraint on the probability of false alarm $\mathbb{P}_0(A_1)$. The challenge for such an optimization is that these probabilities are impossible to express analytically for any nontrivial case of interest. Fortunately, tight upper bounds are known and can be used for the selection of the threshold γ in (2) (Pahlajani et al, 2014b). The approach in this paper, exploits those bounds

to formulate an optimal control problem for the motion of the sensors, and solve this problem analytically.

4 Problem Statement

Assume that the position trajectory of sensor i is controlled through input $u_i(t)$ as in

$$\dot{x}_i = u_i \quad . \quad (3)$$

We assume that there are constraints on control actuation in the form $\|u_i\| \leq u_{\max}$ for some constant $u_{\max} > V_t$, and we collect all sensor motion control inputs in a stack vector $\mathbf{u} = (u_1, \dots, u_{k_s})$. Recall (1), and note that since x_i is implicitly determined by u_i , and ν_i is a function of x_i , ν_i is a functional operating on u_i ; we thus write it as $\nu_i(u_i)$, or more generally $\nu_i(\mathbf{u})$. Define now the scalar quantity

$$\mu_i(\mathbf{u}) \triangleq 1 + \frac{\nu_i(\mathbf{u})}{b_i} \quad . \quad (4)$$

For p being a scalar (control) parameter in $(0, 1)$, it can be shown (Pahlajani et al, 2014b) that the logarithm of an upper bound on the probability of miss $\mathbb{P}_1(\Omega \setminus A_1) = 1 - \mathbb{P}_1(A_1)$ for the fusion center of the network of sensors is analytically expressed as the sum of

$$J_{\text{PM}}(\mathbf{u}, p) \triangleq \sum_{i=1}^{k_s} \int_0^T [\mu_i(\mathbf{u})^p \log \mu_i(\mathbf{u}) - \mu_i(\mathbf{u}) + 1] b_i ds \quad (5)$$

and a constant $\log \alpha$ for $\alpha \in (0, 1)$, while the probability of false alarm is upper bounded by α if

$$F_{\text{FA}}(\mathbf{u}, p) \triangleq \sum_{i=1}^{k_s} \int_0^T [p \mu_i(\mathbf{u})^p \log \mu_i(\mathbf{u}) - \mu_i(\mathbf{u})^p + 1] b_i ds = -\log \alpha \quad . \quad (6)$$

It is therefore natural to formulate an optimal control problem, where J_{PM} is a cost to be optimized with respect to \mathbf{u} and p under constraint (6)—with $\log \alpha$ remaining constant. In this problem, the state of the dynamical system is $\boldsymbol{\mu} \triangleq (\mu_1, \dots, \mu_{k_s})$, implicitly determined by \mathbf{u} in (4) via (1) and (3); specifically,

$$\dot{\mu}_i = \frac{2\chi_i a(x_t - x_i)}{b_i(2\chi_i + \|x_t - x_i\|^2)^2} (u_i - \dot{x}_i) \quad . \quad (7)$$

5 Optimal Sensor Management: Analytic Solutions

The path to an analytic solution starts with transforming the constrained optimal control problem (5)–(6) into an unconstrained one. The first partial result establishes the monotonicity of functional F_{FA} in (6) with respect to the positive parameter p .

Lemma 1 Fix \mathbf{u} . F_{FA} is strictly increasing with p .

Proof Write $\frac{\partial F_{FA}}{\partial p} = \sum_{i=1}^{k_s} \int_0^T p \mu_i^p (\log \mu_i)^2 dt$, and note that it is strictly positive since $\mu_i > 1, p \in (0, 1)$. \square

The next step is to establish the existence of a function from $\boldsymbol{\mu}$ to p .

Lemma 2 The (functional) mapping $\boldsymbol{\mu} \mapsto p$, denoted ϕ , associates to each $\boldsymbol{\mu}$ a unique p .

Proof It follows from Lemma 1 and the Implicit Function Theorem. \square

We henceforth write

$$p = \phi(\boldsymbol{\mu}) . \quad (8)$$

Lemma 3 For all $t_1 \in (0, T]$, it is $\left. \frac{\delta \phi(\boldsymbol{\mu})}{\delta \mu_i} \right|_{t_1} \leq 0$.

Proof Consider first a needle perturbation of the form $\epsilon \delta(t - t_1)$ on coordinate i of $\boldsymbol{\mu}$, yielding a perturbed $\tilde{\boldsymbol{\mu}}$ with component $\mu_i(t) + \epsilon \delta(t - t_1)$; here, $\delta(t - t_1)$ is the Dirac function offset at t_1 and $\epsilon > 0$ a small parameter. Using Taylor expansion on the integrand of $F_{FA}(\boldsymbol{\mu}, p)$ we find

$$F_{FA}(\tilde{\boldsymbol{\mu}}, p) \approx F_{FA}(\boldsymbol{\mu}, p) + b_i \epsilon p^2 \mu_i(t_1)^{p-1} \log \mu_i(t_1) ,$$

from which the first order variation in $F_{FA}(\boldsymbol{\mu}, p)$ due to $\epsilon \delta(t - t_1)$ in μ_i is obtained

$$\begin{aligned} F_{FA}(\tilde{\boldsymbol{\mu}}, p + \delta p) - F_{FA}(\boldsymbol{\mu}, p) \\ = b_i \epsilon p^2 \mu_i(t_1)^{p-1} \log \mu_i(t_1) + \frac{\partial F_{FA}}{\partial p} \delta p, \end{aligned}$$

which is zero because F_{FA} is constrained to $-\log \alpha$ (6). Given Lemma 1:

$$\delta p = - \frac{\epsilon b_i p^2 \mu_i^{p-1} \log \mu_i \Big|_{t_1}}{\sum_{i=1}^k \int_0^T p \mu_i^p \log^2 \mu_i dt} .$$

Rewriting $p = \phi(\boldsymbol{\mu})$, it follows

$$\left. \frac{\delta \phi(\boldsymbol{\mu})}{\delta \mu_i} \right|_{t_1} = \lim_{\epsilon \rightarrow 0} \frac{\delta p}{\epsilon} < 0$$

and the proof is completed. \square

We are now ready to apply the Maximum Principle and extract the optimal motion coordination strategy for each sensor.

Proposition 1 The solution for sensor $i \in \{1, \dots, k_s\}$ to the optimal control problem (5)–(7) within the feasible set $\mathcal{U} = \{\mathbf{u} \in \mathbb{R}^{3k_s} : \|u_i\| \leq u_{\max}\}$ is

$$u_i = \begin{cases} \frac{x_t - x_i}{\|x_t - x_i\|} u_{\max} & x_i \neq x_t \\ \dot{x}_t & x_i = x_t \end{cases} .$$

Proof Given (8), the cost functional is written

$$J_{PM} = \sum_{i=1}^{k_s} \int_0^T (\mu_i^{\phi(\boldsymbol{\mu})} \log \mu_i - \mu_i + 1) b_i dt .$$

Since J_{PM} is always finite, by Fubini's theorem,

$$J_{PM} = \int_0^T \sum_{i=1}^{k_s} (\mu_i^{\phi(\boldsymbol{\mu})} \log \mu_i - \mu_i + 1) b_i dt .$$

The Hamiltonian is

$$H = \sum_{i=1}^{k_s} \lambda_i \dot{\mu}_i(u_i) - \sum_{i=1}^{k_s} (\mu_i^{\phi(\boldsymbol{\mu})} \log \mu_i - \mu_i + 1) b_i \quad (9)$$

and dynamics of costates λ_i is written as

$$\dot{\lambda}_i = - \frac{\partial H}{\partial \mu_i} = (\phi(\boldsymbol{\mu}) \mu_i^{\phi(\boldsymbol{\mu})-1} \frac{\delta \phi(\boldsymbol{\mu})}{\delta \mu_i} \log \mu_i + \mu_i^{\phi(\boldsymbol{\mu})-1} - 1) b_i .$$

Since $\mu_i > 1$ and $\phi(\boldsymbol{\mu}) \in (0, 1)$, we have $0 < \mu_i^{\phi(\boldsymbol{\mu})-1} < 1$, and therefore

$$\dot{\lambda}_i < b_i \mu_i^{\phi(\boldsymbol{\mu})-1} \phi(\boldsymbol{\mu}) \frac{\delta \phi(\boldsymbol{\mu})}{\delta \mu_i} \log \mu_i \stackrel{\text{Lemma 3}}{\leq} 0 \quad (10)$$

for all $t \in (0, T]$.

Now since $\mu_i^*(T)$ can take any value in $(1, 1 + \frac{a}{2b}]$, there are two mutually exclusive and exhaustive cases: either $\mu_i^*(T) \in (1, 1 + \frac{a}{2b})$, or $\mu_i^*(T) = \mu_{i_{\max}} = 1 + \frac{a}{2b}$. If $\mu_i^*(T) \in (1, 1 + \frac{a}{2b})$, the transversality condition requires $\lambda_i(T) = 0$. Thus, given (10), it is $\lambda_i(t) > 0 \quad \forall t \in (0, T]$. In light of this, and given (7), the Hamiltonian maximization condition $H(\boldsymbol{\mu}^*, \mathbf{u}^*, \boldsymbol{\lambda}^*) = \max_{\mathbf{u} \in \mathcal{U}} H(\boldsymbol{\mu}^*, \mathbf{u}^*, \boldsymbol{\lambda}^*)$ applied on (9) requires that

$$u_i^* = \frac{x_t - x_i}{\|x_t - x_i\|} u_{\max} , \quad (11)$$

that is, it suggests the maximal control effort to close the distance between sensor and source as close as possible. Using such a controller, eventually (given big enough T) it will be $\mu_i^*(T) = \mu_{i_{\max}}$. At this point, the second case is in effect. Denote T_s the switching time. Now $t \in [T_s, T]$ with boundary condition $\mu_i(T_s) = \mu_i(T) = \mu_{i_{\max}}$ and $\frac{\delta J_{PM}}{\delta \mu_i} = \dot{\lambda}_i < 0$. To minimize J_{PM} when $t \in [T_s, T]$, μ_i should once again be kept at its maximum value. \square

Essentially what Proposition 1 dictates is for the sensor platforms to close the gap between themselves and the suspected target as fast as possible.

6 Sensor navigation amongst obstacles

Limiting the feasible positions that sensors can attain augments the set of constraints in the optimal control problem formulation (5)–(6). In the general case, the resulting optimal control problem may not admit analytic solutions any more. Even if such solutions can be found, it is conceivable that the optimal controls steer the sensors right at the boundary of the feasible state set, grazing the obstacles in an effort to increase the lower bound on the detection probability. These considerations motivate an alternative, albeit suboptimal, approach to sensor management, which—while adhering to the same principle of closing the distance as quickly as possible—is likely to trade-off some performance for safety and analytically established convergence properties.

Using the insight obtained from the unconstrained case, we therefore develop a sensor management strategy for navigation amongst obstacles in the context of navigation functions. Instead of running at full speed toward the target, sensors will now perform steepest descent over a smooth artificial landscape in which obstacles are regions of high elevation and the target sits surrounded by an area of depression. The latter attribute of this landscape is motivated from the fact that we cannot allow the sensor platforms to physically touch and collide with their target, but rather keep them at a minimum safe distance r_t away from it. The destination for the sensors thus becomes a *set*, the surface of a sphere centered at the moving target. Another technical challenge is that this destination set is time-varying. Inevitably, the convergence problem becomes one where the underlying system is *time-varying*—fully knowing the target’s trajectory is not sufficient to reduce the system into a time-invariant one, because the obstacles are fixed.

For sensor i at position x_i , the goal function that the potential field attempts to minimize takes the form

$$J_i(x_i, t) = (\|x_i - x_t(t)\|^2 - r_t^2)^2 .$$

It can be shown that J_i has two distinct sets of critical points, one isolated point at x_t which is a local maximum, and a manifold of local minima on the boundary of the sphere $\mathcal{B}_{x_t}(r_t)$ defined by $\|x_i - x_t(t)\|^2 - r_t^2 = 0$. We define $\mathcal{B}_{x_t}(\delta_t)$ as a (small) ball around x_t with radius $0 < \delta_t < r_t$. We show later that as long as initial conditions are r_t away from x_t , the stated controller provides convergence to $\partial\mathcal{B}_{x_t}(r_t)$.

So far we have treated the sensors as point masses (negligible volume); we will therefore ignore the possibility of them colliding with each other and focus on steering them away from environment obstacles. In

the spirit of the preliminary sphere-world analysis of [Koditschek and Rimon (1990)], these obstacles are sets \mathcal{O}_j , where $j \in \{1, \dots, m\}$, which are assumed to be open balls in the appropriate Euclidean space (here, \mathbb{R}^3) having radius ρ_j and center o_j . The boundary of obstacle j , for $j \in \{1, \dots, m\}$, is described by means of the function $\beta_{i,j} = \|x_i - o_j\|^2 - \rho_j^2$, which vanishes on the obstacle’s boundary and is positive in the space surrounding it. $\partial\mathcal{O}_0$ marks the outer workspace boundary, of radius ρ_0 ; this boundary is expressed in the form $\beta_{i,0} = \rho_0^2 - \|x_i\|^2$, for $o_0 = 0$. Then a single scalar function that serves as a metric of proximity to (any) obstacle boundary $\beta_i = \prod_{j=0}^M \beta_{i,j}$ can be defined.

Once we “puncture” the interior of workspace boundary with every obstacle, we obtain the *free* workspace $\mathcal{P} = \mathcal{B}(\rho_0) \setminus \bigcup_{j=1}^m \mathcal{O}_j$. Assume that \mathcal{O}_j for $j = \{1 \dots m\}$ are isolated, static, that o_j are at least $\rho_j + r_t$ away from the target $\forall t \in [0, T]$, and that x_t is r_t away from the workspace boundary $\partial\mathcal{O}_0$ —these four requirements correspond to the collision-free workspace remaining *valid* [Koditschek and Rimon (1990)], at least during the sensors’ integration window.

Theorem 1 *Given that the workspace is \mathcal{P} valid, there exists a positive value N such that for every $k \geq N$, the function*

$$\varphi_i(x_i, x_t) = \frac{J_i(x_i, x_t)}{(J_i(x_i, x_t)^k + \beta_i(x_i))^{1/k}} \quad (12)$$

is such that all critical points other than those in $\partial\mathcal{B}_{x_t}(r_t)$ are either nondegenerate with attraction regions of measure zero or in $\mathcal{B}_{x_t}(\delta_t)$, and the gradient field generated by $\nabla_{x_i} \varphi_i$ has $\partial\mathcal{B}_{x_t}(r_t)$ as the only limit set with non-zero measure attraction region outside $\mathcal{B}_{x_t}(\delta_t)$.

Proof The fact that outside $\mathcal{B}_{x_t}(\delta_t)$, φ_i has only local minima on target set $\partial\mathcal{B}_{x_t}(r_t)$, and that all other critical points are non-degenerate (saddle) with measure zero attraction, is established through the series of Propositions 3 through 9 stated and proven in the Appendix. \square

There are some practical considerations related with the application of a bang-bang controller like (11) within a constrained environment, especially when it is undesirable for sensor platforms to collide with their target at maximum speed. Even when the system’s manifold of attractors is set at a safe distance r_t away from the target, flowing along the direction of the negated gradient of (12) at full speed is certain to result in overshoot and oscillatory behavior in the neighborhood of the attracting set. The sensors’ approach to this goal set needs to be fast but gradual. For these reasons, given Theorem 1,

a relaxation on (11) for implementation in constrained environments in the following form is proposed

$$u_i^o = -c \frac{\nabla_{x_i} \varphi_i}{\|\nabla_{x_i} \varphi_i\| + \xi} - (\nabla_{x_t} \varphi_i^T \dot{x}_t) \frac{\nabla_{x_i} \varphi_i}{\|\nabla_{x_i} \varphi_i\|^2}, \quad (13)$$

for some constants $c < u_{\max}$, and $\xi > 0$.

Control law (13) is essentially a modulated (negated) gradient following tracking controller with a feedforward to compensate for target motion. It can be shown that if $\sup_{t \geq 0} \|\dot{x}_t(t)\|$ is sufficiently small compared to u_{\max} , then (c, ξ, ϵ) can be always be chosen so that both (a) $\|u_i^o\| \leq u_{\max}$ for all positions that $\beta_i(x_i) > 0$ except for a small region around saddle points, and (b) (gradual) convergence to the surface of the ball of radius r_t around the target is analytically established. The former claim on the boundedness of (13), relates to lower bounding $\|\nabla_{x_i} \varphi_i\|$ which appears in the denominator of the second term. This term vanishes as x_i approaches one of the critical points of φ_i . For a properly tuned navigation function, those critical points can be expected to be in a set $\bigcup_{j=0}^m \{x_i | \beta_{ij}(x_i) < \epsilon\} \cup \partial \mathcal{B}_{x_t}(r_t) \cup \mathcal{B}_{x_t}(\delta_t)$; we shall prove that under reasonable assumptions² the magnitude of the control input is upper bounded.

Lemma 4 *For x_i sufficiently far from saddle points, u_i^o is bounded.*

Proof Bound $\|u_i^o\|$ as follows

$$\begin{aligned} \|u_i^o\| &= \left\| -c \frac{\nabla_{x_i} \varphi_i}{\|\nabla_{x_i} \varphi_i\| + \epsilon} - (\nabla_{x_t} \varphi_i^T \dot{x}_t) \frac{\nabla_{x_i} \varphi_i}{\|\nabla_{x_i} \varphi_i\|^2} \right\| \\ &\leq c \left\| \frac{\nabla_{x_i} \varphi_i}{\|\nabla_{x_i} \varphi_i\| + \epsilon} \right\| + |\nabla_{x_t} \varphi_i^T \dot{x}_t| \left\| \frac{\nabla_{x_i} \varphi_i}{\|\nabla_{x_i} \varphi_i\|^2} \right\| \\ &< c + \frac{\|\nabla_{x_t} \varphi_i\|}{\|\nabla_{x_i} \varphi_i\|} \|\dot{x}_t\| \\ &= c + \frac{\|k\beta_i \nabla_{x_i} J_i\|}{\|k\beta_i \nabla_{x_i} J_i - J_i \nabla_{x_i} \beta_i\|} \|\dot{x}_t\| \\ &= c + \left(1 + \frac{\|k\beta_i \nabla_{x_i} J_i\| - \|k\beta_i \nabla_{x_i} J_i - J_i \nabla_{x_i} \beta_i\|}{\|k\beta_i \nabla_{x_i} J_i - J_i \nabla_{x_i} \beta_i\|}\right) \|\dot{x}_t\| \\ &\leq c + \left(1 + \frac{\|J_i \nabla_{x_i} \beta\|}{\|k\beta \nabla_{x_i} J_i - J_i \nabla_{x_i} \beta\|}\right) \|\dot{x}_t\|. \end{aligned}$$

The denominator $\|k\beta \nabla_{x_i} J_i - J_i \nabla_{x_i} \beta\|$ vanishes at critical points, i.e., saddle points and the target set.

² We need to note, however, that requiring x_i to be away from saddle points cannot be guaranteed a priori for all initial conditions; there will be a set of initial conditions (Fig. 3) around the attraction regions of the unstable critical points of φ_i that generate trajectories which cross into $\{x_i : 1 + \frac{\|J_i \nabla_{x_i} \beta\|}{\|k\beta \nabla_{x_i} J_i - J_i \nabla_{x_i} \beta\|} \geq \frac{u_{\max} - c}{\max\{\|\dot{x}_t\|\}}\}$.

As x_r is converging to the target set $\partial \mathcal{B}_{x_t}(r_t)$, the upper bound of $\|u_i^o\|$ becomes:

$$\|u_i^o\| < c + \left(1 + \frac{\|\frac{\nabla_{x_i} \beta}{\beta}\|}{\|k\frac{\nabla_{x_i} J_i}{J_i} - \frac{\nabla_{x_i} \beta}{\beta}\|}\right) \|\dot{x}_t\|,$$

and since, by assumption, the target is always away from obstacles, $\|\frac{\nabla_{x_i} \beta}{\beta}\|$ is upper bounded. Therefore,

$$\frac{\|\nabla_{x_i} J_i\|}{J_i} = \frac{4\|x_i - x_t\|}{\|x_i - x_t\|^2 - r_t^2} \xrightarrow{x_i \rightarrow \partial \mathcal{B}_{x_t}(r_t)} +\infty,$$

bounding $\|u_i^o\|$ around the target set and making it converge to $c + \|\dot{x}_t\|$.

If now x_i is close to a saddle point, the control input is still bounded by u_{\max} as long as x_i satisfies

$$x_i \in \left\{x_i : 1 + \frac{\|J_i \nabla_{x_i} \beta\|}{\|k\beta \nabla_{x_i} J_i - J_i \nabla_{x_i} \beta\|} \leq \frac{u_{\max} - c}{\max\{\|\dot{x}_t\|\}}\right\}.$$

The above can be relaxed to

$$\left\{x_i : \|k\beta \nabla_{x_i} J_i - J_i \nabla_{x_i} \beta\| \geq \frac{\max\{\|\dot{x}_t\|\}}{u_{\max} - c - \max\{\|\dot{x}_t\|\}} \sup(J_i \nabla_{x_i} \beta)\right\},$$

where the supremum is taken over $\{x_i : \beta_i(x_i) > 0\}$. Thus, as long as x_i stays sufficiently far away from saddle points, the control input is bounded.

Theorem 2 *The closed loop system (3)–(13) converges to the set $\{x_i \in \mathbb{R}^3 : J_i(x_i, x_t) = 0\}$, from almost everywhere in $\{x_i \in \mathbb{R}^3 : \beta_i(x_i) > 0, x_i \notin \mathcal{B}_{x_t}(r_t), \|x_i\| < \rho_0\}$.*

Proof The closed loop system is time-varying due to $x_t(t)$. The proof is thus based on Barbalat's lemma using function φ_i . The aim is to show that $\lim_{t \rightarrow \infty} \dot{\varphi}_i = 0$.

First note that $\varphi_i \geq 0$. Then expand $\dot{\varphi}_i$ and plug (13) to verify that

$$\dot{\varphi}_i = -c \frac{\|\nabla_{x_i} \varphi_i\|^2}{\|\nabla_{x_i} \varphi_i\| + \xi} \leq 0. \quad (14)$$

So $\lim_{t \rightarrow \infty} \varphi_i$ exists and bounded. Thus according to Barbalat's lemma, proving that $\lim_{t \rightarrow \infty} \dot{\varphi}_i = 0$ reduces to showing that $\dot{\varphi}_i$ is uniformly continuous in t , which can be ensured if $\ddot{\varphi}_i$ is bounded. Toward this end note that

$$\ddot{\varphi}_i = -c \frac{1 - \frac{1}{2} \|\nabla_{x_i} \varphi_i\|}{(\|\nabla_{x_i} \varphi_i\|^2 + \xi)^2} \frac{d\|\nabla_{x_i} \varphi_i\|^2}{dt},$$

and is bounded if $\frac{d\|\nabla_{x_i}\varphi_i\|^2}{dt}$ is. Indeed,

$$\begin{aligned} \frac{d\|\nabla_{x_i}\varphi_i\|^2}{dt} &= -2 \frac{\nabla_{x_i}\varphi_i^\top \nabla_{x_i}^2\varphi_i \nabla_{x_i}\varphi_i}{\|\nabla_{x_i}\varphi_i\| + \xi} \\ &\quad - 2 \frac{\nabla_{x_t}\varphi_i^\top \dot{x}_t}{\|\nabla_{x_i}\varphi_i\|^2} \nabla_{x_i}\varphi_i^\top \nabla_{x_i}^2\varphi_i \nabla_{x_i}\varphi_i \\ &\quad + 2\nabla_{x_i}\varphi_i^\top \nabla_{x_i}(\nabla_{x_t}\varphi_i) \dot{x}_t . \end{aligned}$$

With φ_i being a smooth function, its first and second partial derivatives are bounded on the compact subset of \mathbb{R}^3 where $\beta_i \geq 0$. The second term does not explode because the expression $\left| \frac{\nabla_{x_i}\varphi_i^\top [\nabla_{x_i}^2\varphi_i] \nabla_{x_i}\varphi_i}{\|\nabla_{x_i}\varphi_i\|^2} \right|$ admits an upper bound equal to the maximum eigenvalue of the Hessian of φ_i —which is finite. Therefore, since $\|\dot{x}_t\| < V_t$, $\frac{d\|\nabla_{x_i}\varphi_i\|^2}{dt}$ is bounded, and $\dot{\varphi}_i$ is uniformly continuous, it follows that $\lim_{t \rightarrow \infty} \dot{\varphi}_i = 0$. Then (14) implies that $\lim_{t \rightarrow \infty} \|\nabla_{x_i}\varphi_i\| = 0$, which in turns suggests—based on Theorem 1—that with time $x_i \rightarrow \{x \in \mathbb{R}^3 : J_i(x, x_t) = 0\}$ from almost all initial conditions in $\{x_i \in \mathbb{R}^3 : \beta_i(x_i) > 0, x_i \notin \mathcal{B}_{x_t}(r_t), \|x_i\| < \rho_0\}$, notice that as long as $x_i(0) \notin \mathcal{B}_{x_t(0)}(r_t)$, it will always be $x_i(t) \notin \mathcal{B}_{x_t(t)}(r_t)$ due to $\dot{\varphi} \leq 0$ and φ reaches minimum at $\partial\mathcal{B}_{x_t(t)}(r_t)$. \square

7 Reconciling with platform dynamics

Theorem 2 establishes the convergence properties of the motion controller for platform dynamics (3) in the form of a single integrator. A natural question that arises is what can be said about more complicated sensor platform dynamics. This section demonstrates how different physical sensor platforms can implement the control inputs designed for the single integrator case. This can basically be achieved through application of standard nonlinear system analysis techniques, the first of which is full state, or output, feedback linearization.

In this paper, two types of sensor platforms are considered: a quadrotor, and a wheeled mobile robot. Both systems have full dynamics which afford state–output feedback linearization, with their Cartesian position in the role of the output. Assuming, therefore, that through appropriate input feedback transformations we can now obtain a description of platform i position dynamics in the form of a double integrator with input w_i

$$\ddot{x}_i = w_i , \quad (15)$$

we set off to design an integrator backstepping controller that will realize a desired velocity reference $u_i^\circ = u_i^\circ(x_i, x_t, \dot{x}_t)$ given by the potential field gradient constructed in Section 6. (Note that similar control architectures have been used for convergence to fixed points

[Ayanian et al (2011); Koditschek (1987)].) It follows that for a choice of parameter $k_d > 0$, the input to (15) can be set as

$$w_i = \dot{u}_i^\circ - \nabla_{x_i}\varphi_i - k_d[\dot{x}_i - u_i^\circ] . \quad (16)$$

Proposition 2 *For the closed-loop system (15)–(16), convergence of \dot{x}_i to u_i° is guaranteed.*

Proof First write the error in the reference velocity as $e_v = \dot{x}_i - u_i^\circ$, and express the closed-loop system in the form

$$\begin{aligned} \dot{x}_i &= u_i^\circ + e_v \\ \dot{e}_v &= w_i - \dot{u}_i^\circ . \end{aligned}$$

Consider now the (time-varying) function

$$V(x_i, x_t, e_v) = \varphi_i(x_i, x_t) + \frac{1}{2}e_v^\top e_v$$

and compute

$$\begin{aligned} \dot{V} &= \nabla_{x_i}\varphi_i^\top (u_i^\circ + e_v) + \nabla_{x_t}\varphi_i^\top \dot{x}_t + e_v^\top (w_i - \dot{u}_i^\circ) \\ &= - \frac{\|\nabla_{x_i}\varphi_i\|^2}{\|\nabla_{x_i}\varphi_i\| + \epsilon} + (\nabla_{x_i}\varphi_i + w_i - \dot{u}_i^\circ)^\top e_v \end{aligned}$$

Let the control input w_i to (16) yields

$$\dot{V} = - \frac{\|\nabla_{x_i}\varphi_i\|^2}{\|\nabla_{x_i}\varphi_i\| + \epsilon} - k_d e_v^\top e_v .$$

Application of Barbalat’s lemma along lines parallel to those in Section 6 completes the proof by showing that $\nabla_{x_i}\varphi_i$ and e_v converge to zero with time. The only requirement additional to the treatment of Section 6 is that e_v has to be bounded; this is however, ensured from the negative semidefiniteness of \dot{V} and the positive definiteness of V with respect to x_i and e_v .

8 Numerical and Experimental Assessment

8.1 Simulation study setup

Consider a 2-and-a-half dimensional environment, the projection of which on the 2 dimensional horizontal plane gives the planar workspace topology of Fig. 2. In this environment, a simulated point quadrotor is steered to track a point target moving counterclockwise along a circular path around the origin with angular velocity $\frac{\pi}{5}$ rad per second. Figure 2 compares the performance of this controller in simulation to the results of an experimental study that is discussed later in this section; at this stage we are interested in the thin solid (blue) path in Fig. 2, which corresponds to the simulated vehicle’s trajectory. The target initially starts at point $(x, y) = (0.15, 0)$ m, and in the scenarios shown

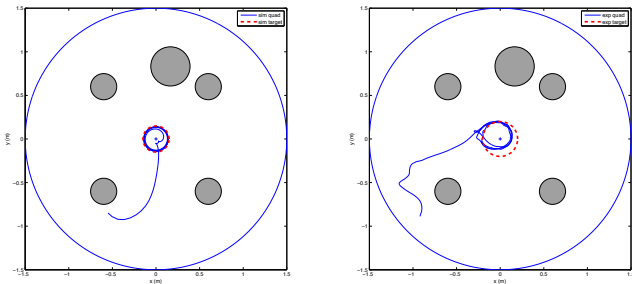


Fig. 2 Simulation (left): a target is circling the origin along a thick red dashed path, and a quadrotor starting from behind an obstacle follows a thin blue solid path as it converges to its target and follows it around in circles. Experiment (right): the same scenario is repeated with a real quadrotor in an experiment where it tracks a simulated target following another circular path with slightly larger radius; here, the path of the quadrotor is marked with a thin solid blue line, while the motion of its target is shown in thick dashed red.

in Fig. 2, it is assumed that the target’s position and velocity are known exactly.

The linear acceleration dynamics of the simulated quadrotor are implemented as in [Mellinger et al (2012)], with the desired roll and pitch angles being part of the control input vector. This model admits feedback linearization and lends itself to implementation of (16). Figure 2 indicates that (16), applied to the quadrotor position dynamics, is capable of achieving target tracking with simultaneous obstacle avoidance.

Although Lemma 4 warns about the existence of trajectories attracted to a neighborhood of saddles, Fig. 3 illustrates that the attraction basin is typically of small measure. Indeed, Fig. 3 marks initial positions from which trajectories cross into

$$\left\{ x_i : 1 + \frac{\|J_i \nabla_{x_i} \beta\|}{\|k\beta \nabla_{x_i} J_i - J_i \nabla_{x_i} \beta\|} \geq \frac{u_{max} - c}{\max\{\|\dot{x}_t\|\}} = 10 \right\} .$$

The marked region shrinks as u_{max} is increased.

8.2 Experimental study setup

Now controller (16) is applied on an AscTek Hummingbird quadrotor, which is supposed to move in a physical environment identical to that of Fig. 2, with the difference that obstacle boundaries are virtual. The target is now following a circular path of radius 0.2 m, with a linear speed of 0.1 m/s. The path followed by the real quadrotor as it tracks its target is shown in Fig. 2 as a dashed-dot curve. While not evident in Fig. 2, the unmodeled (assumed very fast) attitude dynamics of the quadrotor, affect its tracking performance.³ The

³ In fact, the robot’s manufacturer does not give direct access to the attitude control loops; the roll-pitch-yaw angles

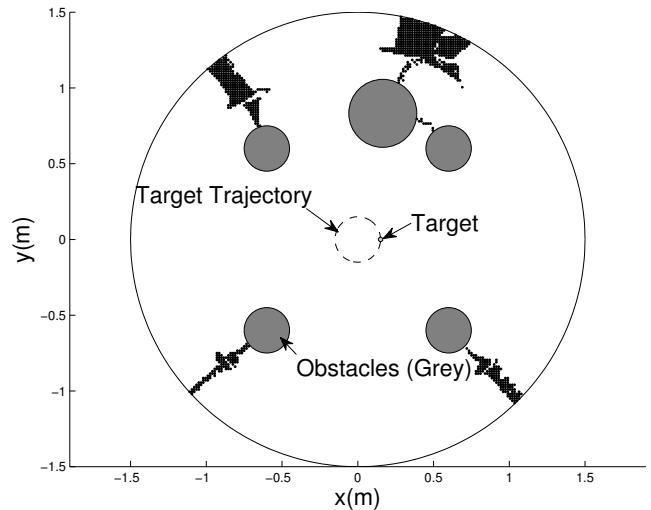


Fig. 3 A graph showing the feasible region (white) and regions requiring velocity references that are 10 times higher than target velocity (black) inside the workspace for a point target following circular trajectory centered at origin with radius $r = 0.15$ and angular velocity $\omega = \pi/5$ that starts at point $(0.15, 0)$.

difference in performance between simulation and experiment, attributed here to the unmodeled attitude dynamics, is shown more clearly in Figs. 4 and 5. Figure 4 shows the distance between the sensor platform and its target over time, in dashed (red) curve for the simulated robot case, and in solid (blue) curve for the actual hardware. The desired distance (clearance) is set at 50 mm, and it is shown as a horizontal (blue) dashed line. Although in both cases, the distance converges to the desired one, the real quadrotor maintains a larger distance error.

are treated as control setpoints by the default firmware on this robot.

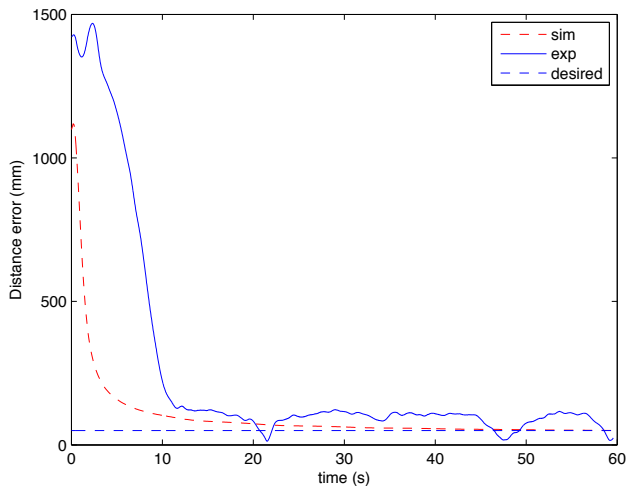


Fig. 4 The distance between target and the quadrotor in the simulation and experimental cases. The horizontal (blue) dashed line is the desired distance to target, while the solid (blue) is the actual distance between target and quadrotor during experiment, and the (red) dashed curve is the distance to the simulated platform.

The reason for the tracking discrepancy in the experimental tests is more apparent in Fig. 5. By ignoring the attitude dynamics, one essentially assumes that the desired roll and pitch angles are attained instantaneously. Figure 5 shows that while the attitude dynamics may be indeed fast, their converging time is not infinitesimal compared to that of position dynamics. A lag in achieving the desired pitch angle, propagates into a lag in linear acceleration, which is then integrated into a velocity error.

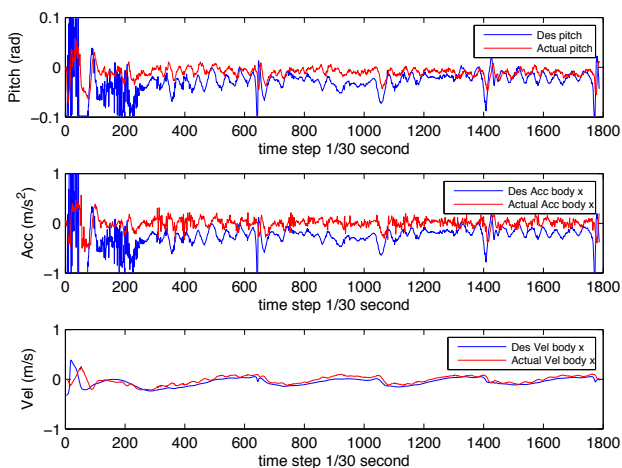


Fig. 5 Comparison between the desired and the actual pitch angle during the flight, and its effect on linear position dynamics.

9 Application to radiation detection

9.1 Experimental Setup

The setup of the experiment where physical sensor platforms are tracking and identifying radioactive sources is depicted in Fig. 6. An AscTek Hummingbird quadrotor and an iCreate wheeled mobile robot are fitted with Geiger counters, and are tasked to detect the presense of a very weak radiation source composed of a small number of vaseline glass (containing Uranium oxide) beads. This source is carried around on a miniature 3D-printed wheg-leg crawling robot, remotely controlled by a human operator. This source is so weakly radioactive, that its perceived intensity drops at a level of less than 10% of ambient background just after 17 cm away. The background radiation level observed by our two sensors during the experiments, ranges from 9.5 to 12.5 counts per minute. In order for detection to be feasible within a time window of 3 minutes, the two sensor platforms have to get close to the target (source), at a distance of less than 10 cm.

The experiment evolves in the same virtual obstacle workspace as the test shown in Fig. 2. Here, the outer workspace boundary is at a radius of 150 cm around the origin of the inertial coordinate frame. The four small (virtual) interior obstacles have a radius of 15 cm, while the single bigger one is of 22.5 cm radius. During the detection task, the two mobile sensor platforms gather radiation count information using their on-board Geiger counters, and at the end of the 3 minute obser-

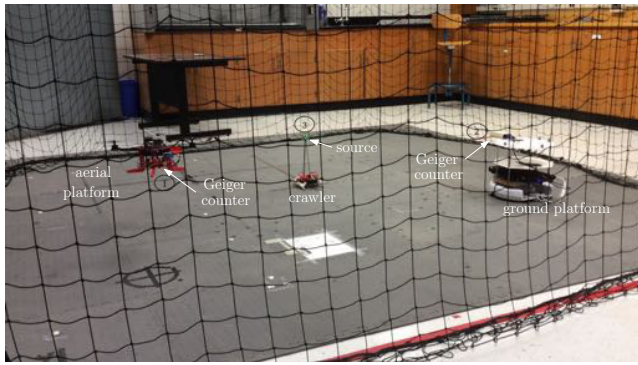


Fig. 6 The radiation detection experiment. Geiger counters are carried by an aerial platform (1) and a ground platform (2), while the weak radiation source (3) moves with a remotely controlled crawling robot.

vation window, they transmit wirelessly their computed statistics to a central computer that performs the likelihood ratio test. The outcome of this test is a decision as to whether the target is radioactive.

Given that for the particular sensor geometry utilized, the cross-section coefficient χ_i is negligible compared to the distance between sensor and source, the perceived source intensity can confidently be approximated as $\nu_i = \frac{\chi_i a}{2\chi_i + r_i^2} \approx \frac{a_i}{r_i^2}$, so that the actual value of the sensor cross-section coefficient is no longer required, and the average of the counts recorded in the unit of time becomes $b_i + \frac{a_i}{r_i^2}$. Figure 7 confirms the validity of this approximation, and illustrates why it is impractical to attempt detection of weak moving radiation sources using stationary counter networks.

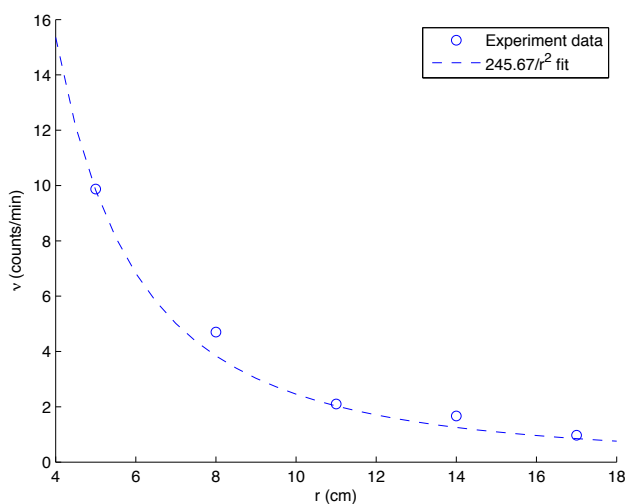


Fig. 7 The perceived source intensity ν_i follows an r^{-2} fall-off. Circles mark radiation measurements made by the Geiger counter mounted on the quadrotor, and the dashed curve corresponds to a $\frac{a_i}{r_i^2}$ fit.

Thus coming as close to the target as possible is key to being able to detect weak radioactive material in motion. The controller constructed closes the distance between sensor and source and maintains it at a desired small setpoint during the detection time window. A motion capture system is used to obtain ground truth information and provide initial target position information to the sensor platforms, while a camera on board the quadrotor uses visual feedback to localize the target while in motion. The target trajectory information obtained through the on-board sensors contains a significant amount of noise; however, the noise in the signal does not prevent the platforms from tracking their target reasonably well (Fig. 8).

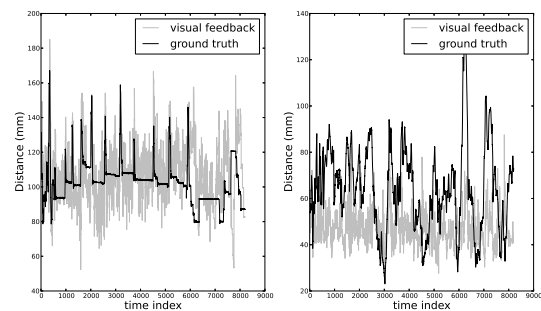


Fig. 8 Distance between sensor platforms—Left ground, Right aerial—and target maintained based on visual feedback against ground truth. The unit of measurement on the time index axis is 0.02 seconds.

Figure 9 shows the paths of the two platforms and their target, moving amidst the virtual obstacles during one of the radiation detection experiments. The dashed (blue) line corresponds to the (projected on the horizontal plane) path of the aerial platform, which returns to the initial landing spot at the end of the 3 minute track-

ing window. The dotted (red) curve marks the path of the wheeled ground platform, while the solid (green) quivering path is that of the source, which wavers somewhat being at the end of a pole fixed on the crawling legged vehicle. Due to the noisy nature of the visual target motion feedback information and the sensitivity of any potential field reference close to an equilibrium configuration, once the platforms achieved the 10 mm target distance objective using (16), they switched to a local PID controller for tracking.

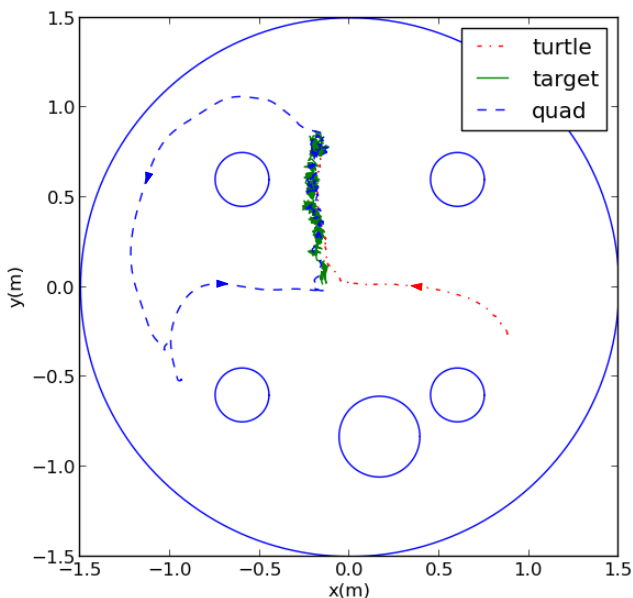


Fig. 9 Superimposed paths of sensor platforms and target during a single radiation detection trial

Fifty radiation detection trials like the one shown in Fig. 9 were conducted, and likelihood ratio tests were performed for a maximum false alarm rate of 1.2 %. Out of the 50 different trials, half were performed with a radiation source on the target, and the other half without it. In all cases where the source was not present on the target, the likelihood ratio test concluded correctly that the target was benign. Out of the 25 cases where the target was carrying a source, one was reported as a false negative, while in the remaining 24 the target was classified correctly.⁴

⁴ This type of behavior is expected, since detection tests of this nature are skewed conservatively on the side of keeping false alarm rates very low. The rationale is that if this is not the case, then human operators will tend to ignore the report of the detection systems.

10 Conclusion

Under certain simplifying assumptions, sensor mobility can be optimally utilized in the context of networks of radiation counters to boost detection performance in low-rate radiation activity detection scenarios. In the problem at hand, the suspected source is mobile, and sensor platforms obtain information about the source's position and velocity either externally or from on-board sensors. Analytic optimal control solutions point to motion coordination strategies that tend to minimize the distance between sensor and suspected source as quickly as possible, resembling bang-bang minimum-time solutions to optimal control problems. Taking this lesson from the analytical, closed-form solutions obtained for sensor motion in unconstrained environments, the paper develops motion planning strategies for sensor coordination and navigation in obstacle environments with bounds on actuation effort. The motion planning methodology is based on gradient descent along potential fields generated by a special type of time-varying navigation functions, and is implemented on the physical platforms by means of standard nonlinear analysis tools. The resulting control laws are feedback-based and reactive to the source's motion, ensuring asymptotic tracking of the mobile source in addition to obstacle avoidance. The control strategy is tested both in simulation on a two-dimensional detection scenario, and in a series of real, three-dimensional radiation detection cases.

References

- Archibold RC, Gladstone R (2013) Truck With Lethal Load Is Recovered in Mexico. *The New York Times*, 2013 Dec. 5, pp. A12
- Ayanian N, Kallem V, Kumar V (2011) Synthesis of feedback controllers for multiple aerial robots with geometric constraints. In: *IEEE/RSJ International Conference on Intelligent Robots and Systems*, San Francisco, California, pp 3126–3131
- Brémaud P (1981) *Point Processes and Queues*. Springer-Verlag
- Brennan S, Mielke A, Torney D (2005) Radioactive source detection by sensor networks. *IEEE Transactions on Nuclear Science* 52:813–819
- Broad WJ (2012) The Nun Who Broke Into the Nuclear Sanctum. *The New York Times*, 2012 Aug. 11, pp. A1
- Byrd R, Moss J, Priedhorsky W, Pura C, Richter G, Saeger K, Scarlett W, Scott S, Wagner R Jr (2005) Nuclear detection to prevent or defeat clandestine nuclear attack. *IEEE Sensors Journal* 5:593–609

Chin JC, Rao NSV, Yau DKY, Shankar M, Yang Y, Hou JC, Srivathsan S, Iyengar S (2010) Identification of low-level point radioactive sources using a sensor network. *The ACM Transactions on Sensor Networks* 7:21:1–21:35

Choudhury S, Scherer S, Singh S (2013) Rrt*-ar: Sampling-based alternate routes planning with applications to autonomous emergency landing of a helicopter. In: *IEEE International Conference on Robotics and Automation*

Dimarogonas DV, Loizou SG, Kyriakopoulos KJ, Zavlanos MM (2006) A feedback stabilization and collision avoidance scheme for multiple independent non-point agents. *Automatica* 42(2):229 – 243

Ghaffarkhah A, Mostofi Y (2009) Communication-aware navigation functions for cooperative target tracking. In: *American Control Conference, St. Louis, Missouri, USA*, pp 1316–1322

Goncalves VM, Pimenta LCA, Maia CA, Dutra BCO, Pereira GAS (2010) Vector fields for robot navigation along time-varying curves in n-dimensions. *IEEE Transactions on Robotics* 26:647–659

Karaman S, Frazzoli E (2011) Sampling-based algorithms for optimal motion planning. *The International Journal of Robotics Research* 30(7):846–894

Koditschek DE (1987) Adaptive techniques for mechanical systems. In: *Fifth Yale Workshop on Applications of Adaptive Systems Theory*, pp 259–265

Koditschek DE, Rimon E (1990) Robot navigation functions on manifolds with boundary. *Advances in Applied Mathematics* 11:412–442

Loizou S, Tanner H, Kumar V, Kyriakopoulos K (2003) Closed loop navigation for mobile agents in dynamic environments. In: *Proceedings of the IEEE/RSJ International Conference on Intelligent Robots and Systems*, vol 4, pp 3769–3774

Marble J, Bekris K (2013) Asymptotically near-optimal planning with probabilistic roadmap spanners. *IEEE Transactions on Robotics* 29(2):432–444

Mellinger D, Michael N, Kumar V (2012) Trajectory generation and control for precise aggressive maneuvers with quadrotors. *The International Journal of Robotics Research* 31:664–674

Nemzek R, Dreicer J, Torney D, Warnock T (2004) Distributed sensor networks for detection of mobile radioactive sources. *IEEE Transactions on Nuclear Science* 51:1693–1700

Pahlajani CD, Poulakakis I, Tanner HG (2014a) Networked decision making for poisson processes with applications to nuclear detection. *IEEE Transactions on Automatic Control* 59:193–198

Pahlajani CD, Sun J, Poulakakis I, Tanner HG (2014b) Error probability bounds for nuclear detection: Im-

proving accuracy through controlled mobility. *Automatica* In print

Perez A, Platt R, Konidaris G, Kaelbling L, Lozano-Pérez T (2012) Lqr-rrt*: Optimal sampling-based motion planning with automatically derived extension heuristics. In: *IEEE International Conference on Robotics and Automation*, pp 2537–2542

Tanner H, Boddu A (2012) Multiagent navigation functions revisited. *IEEE Transactions on Robotics* 28(6):1346–1359, DOI 10.1109/TRO.2012.2210656

Wei H, Lu W, Zhu P, Huang G, Leonard J, Ferrari S (2014) Visibility-based motion planning for active target tracking and localization. In: *Proceedings of the IEEE/RSJ International Conference on Intelligent Robots and Systems, Chicago, Illinois*, pp 76–82

Ziegler J, Stiller C (2009) Spatiotemporal state lattices for fast trajectory planning in dynamic on-road driving scenarios. In: *IEEE/RSJ International Conference on Intelligent Robots and Systems*, pp 1879–1884

Appendix

To simplify notation, we drop the subscript x_i from the expressions of the gradient and hessian of the navigation, with the understanding that all these differentiations are with respect to x_i . Similarly, instead of distinguishing the obstacle and navigation function of agent i by writing β_i and φ_i , we simply refer to it generically as β and φ . We will use the index i to range over obstacles in the environment.

With a slight abuse of notation, we will now think of the free workspace \mathcal{P} as a subset of \mathbb{R}^n (instead of just \mathbb{R}^3); the results established in this section hold irrespectively of the particular value of $n \in \mathbb{N}_+$. Let $\partial\mathcal{S}_T = \{x \in \mathbb{R}^n : \|x - x_t\| = r_t\}$, for a small $\epsilon > 0$ $\mathcal{B}_i(\epsilon) \triangleq \{x \in \mathbb{R}^n : 0 < \beta_i(x) < \epsilon\}$, and (re)define the decomposition of $\overline{\mathcal{P}}$ into sets $\partial\mathcal{F}$, $\mathcal{F}_0(\epsilon)$, $\mathcal{F}_1(\epsilon)$, $\mathcal{F}_2(\epsilon)$ and $\mathcal{W}(\epsilon)$ as follows.

1. the free space boundary

$$\partial\mathcal{F} = \partial\mathcal{P} = \beta^{-1}(0) ;$$

2. the set “near the obstacles”

$$\mathcal{F}_0(\epsilon) \triangleq \bigcup_{i=1}^M \mathcal{B}_i(\epsilon) \setminus \partial\mathcal{S}_T ;$$

3. the set “near the workspace boundary”

$$\mathcal{F}_1(\epsilon) \triangleq \mathcal{B}_0(\epsilon) \setminus (\partial\mathcal{S}_T \cup \mathcal{F}_0(\epsilon)) ;$$

4. the set “away from the obstacles”

$$\mathcal{F}_2(\epsilon) \triangleq \mathcal{P} \setminus (\partial\mathcal{S}_T \cup \partial\mathcal{F} \cup \mathcal{F}_0(\epsilon) \cup \mathcal{F}_1(\epsilon)) .$$

5. the set “away from the obstacles and target”

$$\mathcal{W}(\epsilon) = \mathcal{F}_2(\epsilon) \setminus \mathcal{B}_{x_t}(\delta_t)$$

Recall that a workspace is called *valid*, if the obstacles do not overlap with each other and the destination (set).

Proposition 3 *If the workspace is valid, any $x_d \in \partial\mathcal{S}_T$ is a degenerate local minimum of φ . A vector v satisfying $v^\top \nabla^2 \varphi(x_d) v = 0$ has to be tangent to $\partial\mathcal{S}_T$.*

Proof Evaluate

$$\nabla \varphi(x_d) = \frac{(J^k + \beta)^{1/k} \nabla J - J \nabla (J^k + \beta)^{1/k}}{(J^k + \beta)^{2/k}} \Big|_{x_d}$$

and note that since $J|_{x_d} = 0$ and $\nabla J|_{x_d} = 0$, it is $\nabla \varphi(x_d) = 0$. Now

$$\begin{aligned} \nabla^2 \varphi(x_d) &= \frac{(J^k + \beta)^{1/k} \nabla^2 J - J \nabla^2 (J^k + \beta)^{1/k}}{(J^k + \beta)^{2/k}} \Big|_{x_d} \\ &= \beta^{-1/k} \nabla^2 J \Big|_{x_d} = 8 \beta^{-1/k} (x_d - x_t)(x_d - x_t)^\top. \end{aligned}$$

Consider arbitrary vector $v \in \mathbb{R}^n$ and evaluate the quadratic form

$$\begin{aligned} v^\top \nabla^2 \varphi(x_d) v &= 8 \beta^{-1/k} v^\top (x_d - x_t)(x_d - x_t)^\top v \\ &= 8 \beta^{-1/k} \|v^\top (x_d - x_t)\|^2. \end{aligned}$$

This means that $v^\top \nabla^2 \varphi(x_d) v \geq 0$ with equality if and only if v is normal to $(x_d - x_t)$, that is, when v is tangent to $\partial\mathcal{S}_T$. \square

Proposition 4 *If the workspace is valid, all the critical points of φ are in the interior of the free space.*

Proof Let x_0 be a point in $\partial\mathcal{F}$. Then by definition, $\beta_i(x_0) = 0$ for some $i \in \{0, \dots, M\}$. From the workspace being valid, it follows that $\beta_j > 0$ for all $j \in \{0, \dots, M\}$, $j \neq i$. Then,

$$\begin{aligned} \nabla \varphi(x_d) &= \frac{(J^k + \beta)^{1/k} \nabla J - J \nabla (J^k + \beta)^{1/k}}{(J^k + \beta)^{2/k}} \Big|_{x_0} \\ &= \frac{\nabla J - \frac{1}{k} J^{1-k} (k J^{k-1} \nabla J + \nabla \beta)}{J} \Big|_{x_0} \\ &= -\frac{1}{k} J^{-k} \prod_{j=0, j \neq i}^M \beta_j \nabla \beta_i \neq 0 \end{aligned}$$

which completes the proof. \square

Proposition 5 *For every $\epsilon > 0$ there exists a positive integer $N(\epsilon)$ such that if $k \geq N(\epsilon)$ then there are no critical points of $\frac{J^k}{\beta}$ in $\mathcal{W}(\epsilon)$.*

Proof A sufficient condition for $\frac{J^k}{\beta}$ not having critical points in \mathcal{W} is [Koditschek and Rimon (1990, Proposition 3.4)]

$$k > \frac{J \|\nabla \beta\|}{\beta \|\nabla J\|}.$$

For this, it is sufficient to have

$$k \geq \sup_{\mathcal{W}} \frac{J}{\|\nabla J\|} \sup_{\mathcal{W}} \frac{\|\nabla \beta\|}{\beta} > \frac{J \|\nabla \beta\|}{\beta \|\nabla J\|}.$$

The existence of a finite bound of $\sup_{\mathcal{W}} \frac{J}{\|\nabla J\|} \sup_{\mathcal{W}} \frac{\|\nabla \beta\|}{\beta}$ can be established analytically as follows.

$$\begin{aligned} \sup_{\mathcal{W}} \frac{J}{\|\nabla J\|} &= \sup_{\mathcal{W}} \frac{(\|x - x_t\|^2 - r_t^2)^2}{4\|x - x_t\|^3 - 4r_t^2\|x - x_t\|} \\ &= \sup_{\mathcal{W}} \frac{\|x - x_t\|^2 - r_t^2}{4\|x - x_t\|}. \end{aligned}$$

Since $\|x - x_t\|$ is bounded from below and above in \mathcal{W} , and $\inf_{\mathcal{W}} \|x - x_t\| = \delta_t$, it is ensured that $\sup_{\mathcal{W}} \frac{J}{\|\nabla J\|}$ is finite. For the other bound, we have

$$\begin{aligned} \frac{\|\nabla \beta\|}{\beta} &< \sup_{\mathcal{W}} \frac{\|\nabla \beta\|}{\beta} \\ &\leq \sup_{\mathcal{W}} \sum_{i=0}^M \frac{\|\nabla \beta_i\|}{\beta_i} \\ &\leq \frac{2}{\epsilon} \left[\rho_0 + \sum_{i=1}^M \sup_{\mathcal{W}} \|x - o_i\| \right] \end{aligned} \quad (17)$$

The strict inequality is due to the fact that $\|x\| < \rho_0$ for any point in \mathcal{W} . (17) implies that the $\sup_{\mathcal{W}} \frac{\|\nabla \beta\|}{\beta}$ exists and is bounded. Thus, a choice of a sufficiently large $k \geq N(\epsilon)$ would be

$$N(\epsilon) := \frac{1}{\epsilon} \sup_{\mathcal{W}} \left\{ \frac{\|x - x_t\|^2 - r_t^2}{2\|x - x_t\|} \right\} \left(\rho_0 + \sum_{i=1}^M \sup_{\mathcal{W}} \|x - o_i\| \right). \quad (18)$$

The proof is thus completed. \square

Proposition 6 *For any valid workspace, there exists an $\epsilon_0 > 0$ such that $\frac{J^k}{\beta}$ has no local minima in $\mathcal{F}_0(\epsilon)$, as long as $\epsilon < \epsilon_0$.*

Proof The analysis focuses on $\mathcal{F}_0(\epsilon)$, and that implies that for any critical point $x_c \in \mathcal{F}_0(\epsilon)$, for some i we will have $x_c \in \mathcal{B}_i(\epsilon)$; therefore, $0 < \beta_i(x_c) < \epsilon$. The validity of the workspace guarantees that $\|o_i - x_t\| > r_t + \rho_i$. Because of this, that particular ball $\mathcal{B}_i(\epsilon)$ is bounded away from $\partial\mathcal{S}_T$: for any $x \in \mathcal{B}_i(\epsilon)$, it is $\|x - x_t\| > r_t$ as long as

$$0 < \|x - o_i\| - \rho_i < \sqrt{\epsilon + \rho_i^2} - \rho_i < \|o_i - x_t\| - r_t - \rho_i.$$

Since x_c is a critical point, $k\beta \nabla J = J \nabla \beta$ at x_c . Note that everywhere in $\mathcal{F}_0(\epsilon)$, $J \neq 0$ and $\beta \neq 0$. Therefore, ∇J is aligned with $\nabla \beta$. Using the concept of the omitted product [Koditschek and Rimon (1990)]

$$\bar{\beta}_i \triangleq \prod_{j=0, j \neq i}^M \beta_j$$

vector $\nabla \beta$ expands to

$$\begin{aligned} \nabla \beta &= \sum_{j=1}^M 2(x_c - o_j) \bar{\beta}_j - 2\bar{\beta}_0 x_c \\ &= 2(x_c - o_i) \bar{\beta}_i + 2\beta_i \sum_{j=1, j \neq i}^M (x_c - o_j) \frac{\bar{\beta}_j}{\beta_i} - 2\bar{\beta}_0 x_c \end{aligned}$$

and by defining

$$\alpha_i \triangleq 2 \sum_{j=1, j \neq i}^M (x_c - o_j) \frac{\bar{\beta}_j}{\beta_i} - 2\frac{\bar{\beta}_0}{\beta_i} x_c$$

which is a vector independent from ϵ , and bounded in $\mathcal{F}_0(\epsilon)$, one has

$$\nabla \beta = 2(x_c - o_i) \bar{\beta}_i + \beta_i \alpha_i .$$

From $k\beta \nabla J = J \nabla \beta$ at x_c it now follows that

$$\begin{aligned} \nabla J &= \frac{J}{k\beta} \nabla \beta \\ \iff 4(\|x_c - x_t\|^2 - r_t^2)(x_c - x_t) &= \frac{J}{k\beta} [2(x_c - o_i) \bar{\beta}_i + \beta_i \alpha_i] \end{aligned}$$

which leads to

$$x_c - x_t = \frac{\|x_c - x_t\|^2 - r_t^2}{4} \left(2\frac{x_c - o_i}{k\beta_i} + \frac{\alpha_i}{k\beta_i} \right). \quad (19)$$

If one now sets

$$C_k \triangleq \sup_{\mathcal{W}} \left\{ \frac{\|x_c - x_t\|^2 - r_t^2}{2\|x_c - x_t\|} \right\} \left(\rho_0 + \sum_{i=1}^M \sup_{\mathcal{W}} \|x_c - o_i\| \right)$$

then according to (18) in the proof of Proposition 5, a suitable choice of k would be

$$k := \frac{C_k}{\epsilon}$$

in which case (19) becomes

$$x_c - x_t = \frac{\epsilon(\|x_c - x_t\|^2 - r_t^2)}{4C_k} \left(2\frac{x_c - o_i}{\beta_i} + \frac{\alpha_i}{\beta_i} \right). \quad (20)$$

Taking the inner product of both sides of $k\beta \nabla J = J \nabla \beta$ with ∇J yields

$$\begin{aligned} k\beta \nabla J^\top \nabla J &= J \nabla \beta^\top \nabla J \\ \implies k\beta &= \frac{\bar{\beta}_i \nabla \beta_i^\top \nabla J + \beta_i \nabla \bar{\beta}_i^\top \nabla J}{16\|x_c - x_t\|^2} \quad (21) \end{aligned}$$

From this point, one can then prove that the critical point of $\frac{J^k}{\beta}$ is not a local minimum by showing that $\nabla^2 \frac{J^k}{\beta}$ has at least one negative eigenvalue at that point. (The procedure follows the exact same steps as [Koditschek and Rimon (1990, Proposition 3.6)].) Essentially, it amounts to using any vector \hat{v} orthogonal to $\frac{\nabla \beta_i}{\|\nabla \beta_i\|}$ as a test vector, and showing that at x_c and for small enough ϵ , $\hat{v}^\top \nabla^2 \frac{J^k}{\beta} \hat{v} < 0$. The process in detail is as follows:

$$\begin{aligned} \frac{\beta^2}{J^{k-1}} \hat{v}^\top \nabla^2 \frac{J^k}{\beta} \Big|_{x_c} \hat{v} &= k\beta \hat{v}^\top \nabla^2 J \hat{v} - 2J \bar{\beta}_i \\ &+ \hat{v}^\top J \beta_i \left[\frac{1 - \frac{1}{k}}{\bar{\beta}_i} \nabla \bar{\beta}_i \nabla \bar{\beta}_i^\top - \nabla^2 \bar{\beta}_i \right] \hat{v} \\ (21) \quad \bar{\beta}_i \nabla \beta_i^\top \nabla J + \beta_i \nabla \bar{\beta}_i^\top \nabla J & \hat{v}^\top \nabla^2 J \hat{v} - 2J \bar{\beta}_i \\ & \frac{16\|x_c - x_t\|^2}{} \\ &+ \hat{v}^\top J \beta_i \left[\frac{1 - \frac{1}{k}}{\bar{\beta}_i} \nabla \bar{\beta}_i \nabla \bar{\beta}_i^\top - \nabla^2 \bar{\beta}_i \right] \hat{v} \\ &= \bar{\beta}_i \left(\frac{\hat{v}^\top \nabla^2 J \hat{v}}{16\|x_c - x_t\|^2} \nabla \beta_i^\top \nabla J - 2J \right) \\ &+ \beta_i \left(\frac{\hat{v}^\top \nabla^2 J \hat{v}}{16\|x_c - x_t\|^2} \nabla \bar{\beta}_i^\top \nabla J \right. \\ & \left. + J \hat{v}^\top \left[\frac{1 - \frac{1}{k}}{\bar{\beta}_i} \nabla \bar{\beta}_i \nabla \bar{\beta}_i^\top - \nabla^2 \bar{\beta}_i \right] \hat{v} \right). \quad (22) \end{aligned}$$

To determine the sign of the far right side of (22), perform the expansion of $\hat{v}^\top \nabla^2 J \hat{v}$ into

$$\begin{aligned} \hat{v}^\top [4(\|x_c - x_t\|^2 - r_t^2) \mathbf{I} + 8(x_c - x_t)(x_c - x_t)^\top] \hat{v} \\ = 4(\|x_c - x_t\|^2 - r_t^2) + 8 \hat{v}^\top (x_c - x_t)(x_c - x_t)^\top \hat{v} \\ = 4(\|x_c - x_t\|^2 - r_t^2) + 8(\hat{v}^\top (x_c - x_t))^2, \quad (23) \end{aligned}$$

where \mathbf{I} denotes the identity matrix, and plug (20) into (23), to express $\hat{v}^\top \nabla^2 J \hat{v}$ in the form

$$\begin{aligned} 4(\|x_c - x_t\|^2 - r_t^2) + \\ + 8 \left| \hat{v}^\top \frac{\epsilon(\|x_c - x_t\|^2 - r_t^2)}{4C_k} \left(2\frac{x_c - o_i}{\beta_i} + \frac{\alpha_i}{\beta_i} \right) \right|^2 \\ = 4\sqrt{J} + \frac{2\epsilon\sqrt{J} |\hat{v}^\top \alpha_i|^2}{C_k \bar{\beta}_i}. \quad (24) \end{aligned}$$

where $\hat{v}^\top (x_c - o_i) = 0$ and \sqrt{J} is substituted for $\|x_c - x_t\|^2 - r_t^2$ (for brevity), since in $\mathcal{F}_0(\epsilon)$ it holds $\|x_c - x_t\| > r_t$.

Given now that the second term in (22) can be made arbitrarily small by choosing $\epsilon > \beta_i$, one can establish the negative definiteness of (22) by ensuring that the first term is strictly below zero. The second factor in

the first term in (22) can be expanded

$$\begin{aligned}
& \frac{\hat{v}^\top \nabla^2 J \hat{v}}{16\|x_c - x_t\|^2} \nabla \beta_i^\top \nabla J - 2J \\
& \stackrel{(24)}{=} \frac{2\sqrt{J} + \frac{\epsilon\sqrt{J}}{C_k\bar{\beta}_i} |\hat{v}^\top \alpha_i|^2}{8\|x_c - x_t\|^2} 2(x_c - o_i) 4(x_c - x_t)\sqrt{J} - 2J \\
& = 2J \left[\frac{(x_c - o_i)^\top (x_c - x_t)}{\|x_c - x_t\|^2} - 1 \right] + \\
& + \frac{\epsilon J |\hat{v}^\top \alpha_i|^2}{C_k \bar{\beta}_i \|x_c - x_t\|^2} (x_c - o_i)^\top (x_c - x_t) \\
& = \frac{2J(x_t - o_i)^\top (x_c - x_t)}{\|x_c - x_t\|^2} + \frac{\epsilon J |\hat{v}^\top \alpha_i|^2 (x_c - o_i)^\top (x_c - x_t)}{C_k \bar{\beta}_i \|x_c - x_t\|^2}
\end{aligned}$$

and by applying known relations [Koditschek and Rimon (1990, Lemma 3.5)] one arrives at

$$\begin{aligned}
& \frac{\hat{v}^\top \nabla^2 J \hat{v}}{16\|x_c - x_t\|^2} \nabla \beta_i^\top \nabla J - 2J \\
& \leq \frac{2J\|x_t - o_i\| (\sqrt{\epsilon + \rho_i^2} - \|x_t - o_i\|)}{\|x_c - x_t\|^2} \\
& + \epsilon \sup_{\mathcal{F}_0(\epsilon)} \frac{J |\hat{v}^\top \alpha_i|^2 (x_c - o_i)^\top (x_c - x_t)}{C_k \bar{\beta}_i \|x_c - x_t\|^2} . \quad (25)
\end{aligned}$$

At this point, (25) is used in (22) to upper bound the left hand side of (22)

$$\begin{aligned}
& \frac{\beta^2}{J^{k-1}} \hat{v}^\top \nabla^2 \frac{J^k}{\beta} \Big|_{x_c} \hat{v} \\
& \leq \frac{2J\bar{\beta}_i \|x_t - o_i\| (\sqrt{\epsilon + \rho_i^2} - \|x_t - o_i\|)}{\|x_c - x_t\|^2} \\
& + \epsilon \left(\bar{\beta}_i \sup_{\mathcal{F}_0(\epsilon)} \frac{J |\hat{v}^\top \alpha_i|^2 (x_c - o_i)^\top (x_c - x_t)}{C_k \bar{\beta}_i \|x_c - x_t\|^2} \right. \\
& + \frac{\hat{v}^\top \nabla^2 J \hat{v}}{16\|x_c - x_t\|^2} \nabla \bar{\beta}_i^\top \nabla J \\
& \left. + J \hat{v}^\top \left[\frac{1-\frac{1}{k}}{\beta_i} \nabla \bar{\beta}_i \nabla \bar{\beta}_i^\top - \nabla^2 \bar{\beta}_i \right] \hat{v} \right) .
\end{aligned}$$

Now choosing ϵ appropriately small, the second term can be made sufficiently small so that the sign of the first term dominates. The sign of the latter is determined by the expression $\sqrt{\epsilon + \rho_i^2} - \|x_t - o_i\|$, which for small ϵ approaches $\rho_i - \|x_t - o_i\|$, which is guaranteed negative by the validity of the workspace. (The target x_t is $(r_t + \rho_i)$ away from the center of obstacle i .) \square

Proposition 7 *If $k \geq \frac{C_k}{\epsilon}$, then there exists an $\epsilon_1 > 0$ such that $\hat{\varphi} = \frac{J^k}{\beta}$ has no critical points on $\mathcal{F}_1(\epsilon)$, as long as $\epsilon < \epsilon_1$.*

Proof The set $\mathcal{F}_1(\epsilon)$ expresses the neighborhood of the workspace (outer) boundary. Select ϵ small enough so

that the $\mathcal{B}_0(\epsilon)$ neighborhood of the outer boundary is disjoint from the r_t -neighborhood of the target: $\beta_0 < \epsilon < \rho_0^2 - (\|x_t\| + r_t)^2$. Then any critical point $x_c \in \mathcal{F}_1(\epsilon)$ will satisfy $\beta_0(x_c) = \rho_0^2 - \|x_c\|^2 < \epsilon$, implying $\|x_c\| > \|x_t\| + r_t$. Then in $\mathcal{B}_0(\epsilon)$

$$\begin{aligned}
\nabla J^\top \nabla \beta_0 & = 4(\|x_c - x_t\|^2 - r_t^2)(x_c - x_t)^\top (-2x_c) \\
& = 8(\|x_c - x_t\|^2 - r_t^2)(x_t^\top x_c - \|x_c\|^2) \\
& \leq 8(\|x_c - x_t\|^2 - r_t^2)(\|x_c\| \|x_t\| - \|x_c\|^2) \\
& = 8(\|x_c - x_t\|^2 - r_t^2) \|x_c\| (\|x_t\| - \|x_c\|) \\
& < 0 .
\end{aligned}$$

By choosing ϵ small enough, we can ensure that $\nabla \hat{\varphi}$ does not vanish in $\mathcal{F}_1(\epsilon)$. Here is why:

$$\begin{aligned}
\nabla \hat{\varphi}^\top \nabla J & = \left[\frac{kJ^{k-1}}{\beta} \nabla J - \frac{J^k}{\beta^2} \nabla \beta \right]^\top \nabla J \\
& = \frac{J^k (16k\beta \|x_c - x_t\|^2 - \nabla \beta^\top \nabla J)}{\beta^2} \\
& = \frac{J^k [16k\beta \|x_c - x_t\|^2 - (\beta_0 \nabla \bar{\beta}_0^\top \nabla J + \bar{\beta}_0 \nabla \beta_0^\top \nabla J)]}{\beta^2} \\
& \stackrel{(\nabla J^\top \nabla \beta_0 < 0)}{>} \frac{J^k \beta_0 (16k\bar{\beta}_0 \|x_c - x_t\|^2 - \nabla \bar{\beta}_0^\top \nabla J)}{\beta^2}
\end{aligned}$$

and thus any ϵ small enough to make $k > \frac{\nabla \bar{\beta}_0^\top \nabla J}{16\bar{\beta}_0 \|x_c - x_t\|^2}$, will also make $\nabla \hat{\varphi}^\top \nabla J$ positive. In fact, the choice utilized earlier, i.e., $k = \frac{C_k}{\epsilon}$ suffices. To see this,

$$\begin{aligned}
\frac{\nabla \bar{\beta}_0^\top \nabla J}{16\bar{\beta}_0 \|x_c - x_t\|^2} & \leq \frac{\|\nabla \bar{\beta}_0\| \|\nabla J\|}{16\bar{\beta}_0 \|x_c - x_t\|^2} = \frac{\sqrt{J} \sum_{i=1}^M \bar{\beta}_i \|\nabla \beta_i\|}{4\|x_c - x_t\|} \\
& < \frac{1}{\epsilon} \sup_{\mathcal{W}} \left\{ \frac{\sqrt{J}}{2\|x_c - x_t\|} \right\} \sum_{i=1}^M \sup_{\mathcal{W}} \|x_c - o_i\| ,
\end{aligned}$$

and compare to

$$\begin{aligned}
k := \frac{C_k}{\epsilon} & = \frac{1}{\epsilon} \sup_{\mathcal{W}} \left\{ \frac{\sqrt{J}}{2\|x_c - x_t\|} \right\} \left(\rho_0 + \sum_{i=1}^M \sup_{\mathcal{W}} \|x_c - o_i\| \right) \\
& > \frac{1}{\epsilon} \sup_{\mathcal{W}} \left\{ \frac{\sqrt{J}}{2\|x_c - x_t\|} \right\} \sum_{i=1}^M \sup_{\mathcal{W}} \|x_c - o_i\| .
\end{aligned}$$

It thus suffices to pick $\epsilon < \epsilon_1 = (\rho_0)^2 - (\|x_t\| + r_t)^2$ to ensure that no critical points are in $\mathcal{F}_1(\epsilon)$. \square

Proposition 8 *Critical points in the interior of $\mathcal{F}_0(\epsilon)$ are non-degenerate.*

Proof One way to establish such a claim [Koditschek and Rimon (1990, Proposition 3.9)] is to partition the tangent space of $\hat{\varphi}$ into a subspace that yields positive values for the quadratic form constructed with

$\nabla^2 \hat{\varphi}$, and a subset that yields negative values. The negative case is established by Proposition 6. The positive case, again along the lines of [Koditschek and Rimon (1990, Proposition 3.9)], is established here by taking a test direction $\widehat{\nabla \beta}_i = \frac{\nabla \beta_i}{\|\nabla \beta_i\|}$, and picking ϵ small enough to obtain $\widehat{\nabla \beta}_i^\top \nabla^2 \hat{\varphi} \widehat{\nabla \beta}_i > 0$. Note that for a given i , $\widehat{\nabla \beta}_i$ defines one subspace, and all the vectors \hat{v} form its orthogonal complement. To verify the sign of $\widehat{\nabla \beta}_i^\top \nabla^2 \hat{\varphi} \widehat{\nabla \beta}_i$, expand the expression

$$\begin{aligned} & \frac{\beta^2}{J^{k-1}} \widehat{\nabla \beta}_i^\top \nabla^2 \hat{\varphi} \widehat{\nabla \beta}_i = \\ & = \widehat{\nabla \beta}_i^\top k\beta \nabla^2 J \widehat{\nabla \beta}_i \\ & + \frac{J(1-\frac{1}{k})}{\beta} (\nabla \beta^\top \widehat{\nabla \beta}_i)^2 - J \widehat{\nabla \beta}_i^\top \nabla^2 \beta \widehat{\nabla \beta}_i . \end{aligned} \quad (26)$$

We know [Koditschek and Rimon (1990, Proposition 3.9)] that for small enough ϵ ,

$$\frac{J\|\nabla \beta\|^2}{2k\beta} + \frac{J(1-\frac{1}{k})}{\beta} (\nabla \beta^\top \widehat{\nabla \beta}_i)^2 - J \widehat{\nabla \beta}_i^\top \nabla^2 \beta \widehat{\nabla \beta}_i > 0$$

And although different J function is used here, the same derivation in [Koditschek and Rimon (1990, Proposition 3.9)] holds here. So to set the sign of (26), it suffices to make

$$\widehat{\nabla \beta}_i^\top k\beta \nabla^2 J \widehat{\nabla \beta}_i \geq \frac{J\|\nabla \beta\|^2}{2k\beta} \quad (27)$$

Recalling (23), and that $\|x_c - x_t\|^2 - r_t^2 = \sqrt{J}$ since x_c is a critical point, the left hand side of (27) is

$$\widehat{\nabla \beta}_i^\top k\beta \nabla^2 J \widehat{\nabla \beta}_i = 4k\beta\sqrt{J} + 8k\beta |\widehat{\nabla \beta}_i^\top (x_c - x_t)|^2 \quad (28)$$

and because x_c is a critical point, taking squared norms of both sides of $k\beta \nabla J = J \nabla \beta$ yields

$$(4k\beta\sqrt{J} \|x_c - x_t\|)^2 = J^2 \|\nabla \beta\|^2$$

from which one extracts that

$$4k\beta = \frac{J\|\nabla \beta\|^2}{4k\beta\|x_c - x_t\|^2} . \quad (29)$$

Plugging now (29) back into (28) yields

$$\begin{aligned} & \widehat{\nabla \beta}_i^\top k\beta \nabla^2 J \widehat{\nabla \beta}_i = \\ & \frac{J^{3/2} \|\nabla \beta\|^2}{4k\beta\|x_c - x_t\|^2} + \frac{J\|\nabla \beta\|^2 |\widehat{\nabla \beta}_i^\top (x_c - x_t)|^2}{2k\beta\|x_c - x_t\|^2} . \end{aligned}$$

Now (27) takes the form

$$\begin{aligned} & \frac{J^{3/2} \|\nabla \beta\|^2}{4k\beta\|x_c - x_t\|^2} + \frac{J\|\nabla \beta\|^2 |\widehat{\nabla \beta}_i^\top (x_c - x_t)|^2}{2k\beta\|x_c - x_t\|^2} \geq \frac{J\|\nabla \beta\|^2}{2k\beta} \\ \Leftrightarrow & \frac{J^{1/2}}{2\|x_c - x_t\|^2} + \frac{|\widehat{\nabla \beta}_i^\top (x_c - x_t)|^2}{\|x_c - x_t\|^2} \geq 1 \\ \Leftrightarrow & \frac{\|x_c - x_t\|^2 - r_t^2 + 2 |\widehat{\nabla \beta}_i^\top (x_c - x_t)|^2}{2\|x_c - x_t\|^2} \geq 1 \\ \Leftrightarrow & 2 |\widehat{\nabla \beta}_i^\top (x_c - x_t)|^2 \geq \|x_c - x_t\|^2 + r_t^2 \end{aligned} \quad (30)$$

For $x_c \in \mathcal{B}_i(\epsilon)$ (guaranteed by Proposition 6), $\|x_c - x_t\| > r_t$. Now let r_t assume the form $r_t = \zeta \inf_{\mathcal{B}_i(\epsilon)} \|x_c - x_t\|$ for an appropriate $\zeta < 1$, and recall that $\widehat{\nabla \beta}_i = \frac{\nabla \beta_i}{\|\nabla \beta_i\|}$, where $\nabla \beta_i = 2(x - o_i)$. With this in mind, one satisfies (30) by ensuring that

$$\begin{aligned} \frac{1 + \zeta^2}{2} & \leq \left(\frac{(x_c - o_i)^\top (x_c - x_t)}{\|x_c - o_i\| \|x_c - x_t\|} \right)^2 \\ \Rightarrow & 2 |\widehat{\nabla \beta}_i^\top (x_c - x_t)|^2 \geq \|x_c - x_t\|^2 + r_t^2 . \end{aligned} \quad (31)$$

An appropriately small choice of ϵ can establish (31), as the following derivation shows:

$$\begin{aligned} & \frac{(x_c - o_i)^\top (x_c - x_t)}{\|x_c - o_i\| \|x_c - x_t\|} \geq \\ & \frac{\frac{\sqrt{J}}{4k} [(2\|x_c - o_i\|^2)/\beta_i + [\alpha_i^\top (x_c - o_i)]/\bar{\beta}_i]}{\frac{\sqrt{J}}{4k} [(2\|x_c - o_i\|)/\beta_i + \|\alpha_i\|/\bar{\beta}_i] \|x_c - o_i\|} \\ & \geq \frac{(2\|x_c - o_i\|^2)/\beta_i - (\|\alpha_i\| \|x_c - o_i\|)/\bar{\beta}_i}{(2\|x_c - o_i\|^2)/\beta_i + (\|\alpha_i\| \|x_c - o_i\|)/\bar{\beta}_i} \\ & = \frac{1 - (\beta_i \|\alpha_i\|)/(2\bar{\beta}_i \|x_c - o_i\|)}{1 + (\beta_i \|\alpha_i\|)/(2\bar{\beta}_i \|x_c - o_i\|)} \\ & = 1 - \frac{(\beta_i \|\alpha_i\|)/(\bar{\beta}_i \|x_c - o_i\|)}{1 + (\beta_i \|\alpha_i\|)/(2\bar{\beta}_i \|x_c - o_i\|)} \\ & \geq 1 - \frac{\beta_i \|\alpha_i\|}{\bar{\beta}_i \|x_c - o_i\|} \geq 1 - \frac{\epsilon \|\alpha_i\|}{\bar{\beta}_i \|x_c - o_i\|} \end{aligned}$$

and thus to satisfy (27), it suffices to pick

$$\begin{aligned} \epsilon & < \left(1 - \sqrt{\frac{1 + \zeta^2}{2}} \right) \frac{\inf_i \rho_i^m}{\sup_{\mathcal{F}_0(\epsilon)} \|\alpha_i\|} \\ \Rightarrow & \epsilon < \left(1 - \sqrt{\frac{1 + \zeta^2}{2}} \right) \frac{\bar{\beta}_i \|x_c - o_i\|}{\|\alpha_i\|} \end{aligned}$$

□

Proposition 9 *There exists $k_0 > 0$ such that for any $k > k_0$, any critical point $x_c \in \mathcal{B}_{x_i}(\delta_t)$ is a local maximum of $\frac{J}{\beta}$.*

Proof To study the critical points in $\mathcal{B}_{x_t}(\delta_t)$, we work on the two cases:

Case I: $\nabla\beta|_{x_t} = 0$, $x_c = x_t$,

$\nabla J|_{x_t} = 0 \Rightarrow k\beta(x_t)\nabla J|_{x_t} = J(x_t)\nabla\beta|_{x_t} = 0$, we shall have x_t as one of the critical points in $\mathcal{B}_{x_t}(\delta_t)$. In this case, for any unit vector $q \in \mathbb{R}^n$:

$$\begin{aligned} & \frac{\beta^2}{J^{k-2}} q^\top \nabla^2 \left(\frac{J^k}{\beta} \right) |_{x_t} q \\ &= q^\top (k\beta J \nabla^2 J + k(k-1)\beta \nabla J \nabla J^\top - J^2 \nabla^2 \beta) q \\ &= q^\top (-4J^{1.5} k \beta \mathbf{I} - J^2 \nabla^2 \beta) q \\ &= -4r_t^6 k \beta - r_t^8 q^\top \nabla^2 \beta q \end{aligned}$$

Recall that to make the workspace valid, $\mathcal{B}_{x_t}(r_t)$ should not intersect $\partial\mathcal{F}$, then at x_t , $\beta_i > r_t^2$ for $i \in \{0 \dots m\} \Rightarrow \beta > r_t^{2m}$. So as long as

$$k > k_1 = \frac{1}{4} r_t^{(2-2m)} \sup_q (|q^\top \nabla^2 \beta q|)$$

$q^\top \nabla^2 \left(\frac{J^k}{\beta} \right) |_{x_t} q$ is guaranteed to be negative for any unit vector $q \in \mathbb{R}^n$ and the critical point x_t is a local maximum of $\frac{J^k}{\beta}$.

Case II: For any $x_c \neq x_t, x_c \in \mathcal{B}_{x_t}(\delta_t)$:

For any unit vector $q \in \mathbb{R}^n$, q can be presented as scaled sum of $v_1 = \frac{\nabla J}{\|\nabla J\|}$ and v_2 , a unit vector perpendicular to v_1 , i.e. $q = q_1 v_1 + q_2 v_2, q_1^2 + q_2^2 = 1, q_1 q_2 > 0$. In order to ensure that $\nabla^2 \left(\frac{J^k}{\beta} \right)$ is negative definite at x_c , a critical point of $\frac{J^k}{\beta}$ in $\mathcal{B}_{x_t}(\delta_t)$, we study the sign of $\frac{\beta^2}{J^{k-2}} q^\top \nabla^2 \left(\frac{J^k}{\beta} \right) |_{x_c} q$:

$$\begin{aligned} & \frac{\beta^2}{J^{k-2}} q^\top \nabla^2 \left(\frac{J^k}{\beta} \right) |_{x_c} q \\ &= \frac{\beta^2}{J^{k-2}} \left(q_1^2 v_1^\top \nabla^2 \left(\frac{J^k}{\beta} \right) |_{x_c} v_1 + q_2^2 v_2^\top \nabla^2 \left(\frac{J^k}{\beta} \right) |_{x_c} v_2 + \right. \\ & \quad \left. q_1 q_2 v_1^\top \nabla^2 \left(\frac{J^k}{\beta} \right) |_{x_c} v_2 + q_1 q_2 v_2^\top \nabla^2 \left(\frac{J^k}{\beta} \right) |_{x_c} v_1 \right) \quad (32) \end{aligned}$$

Recall that at critical point x_c , $k\beta \nabla J = J \nabla \beta$. Take the norm of both side:

$$\begin{aligned} k\beta(4J^{0.5}\|x_c - x_t\|) &= J\|\nabla\beta\| \\ k\|x_c - x_t\| &= J^{0.5} \frac{\|\nabla\beta\|}{4\beta} \quad (33) \end{aligned}$$

The first term in (32) can be expanded as:

$$\begin{aligned} & q_1^2 \frac{\beta^2}{J^{k-2}} v_1^\top \nabla^2 \left(\frac{J^k}{\beta} \right) |_{x_c} v_1 \\ &= q_1^2 v_1^\top (k\beta J \nabla^2 J + k(k-1)\beta \nabla J \nabla J^\top - J^2 \nabla^2 \beta) v_1 \\ &= q_1^2 v_1^\top (k\beta J [8(x_c - x_t)(x_c - x_t)^\top - 4J^{0.5} \mathbf{I}] + \dots \\ & \quad + k(k-1)\beta \nabla J \nabla J^\top - J^2 \nabla^2 \beta) v_1 \\ &= q_1^2 (8k(2k-1)\beta J \|x_c - x_t\|^2 - 4k\beta J^{1.5} - J^2 v_1^\top \nabla^2 \beta v_1) \\ &\stackrel{(33)}{=} q_1^2 \left(\frac{J^2 \|\nabla\beta\|^2}{\beta} - 2J^{1.5} \|\nabla\beta\| \|x_c - x_t\| - J^2 v_1^\top \nabla^2 \beta v_1 - \dots \right. \end{aligned}$$

$$\begin{aligned} & \left. - 4k\beta J^{1.5} \right) \\ &\leq q_1^2 \left(\frac{J^2 \|\nabla\beta\|^2}{\beta} - J^2 v_1^\top \nabla^2 \beta v_1 - 4k\beta J^{1.5} \right) \end{aligned}$$

Since v_2 is an arbitrary unit vector that is perpendicular to ∇J , it is also perpendicular to $(x_c - x_t)$. The second term in (32) can be expanded as:

$$\begin{aligned} & q_2^2 \frac{\beta^2}{J^{k-2}} v_2^\top \nabla^2 \left(\frac{J^k}{\beta} \right) |_{x_c} v_2 \\ &= q_2^2 v_2^\top (k\beta J \nabla^2 J + k(k-1)\beta \nabla J \nabla J^\top - J^2 \nabla^2 \beta) v_2 \\ &= q_2^2 v_2^\top (k\beta J [8(x_c - x_t)(x_c - x_t)^\top - 4J^{0.5} \mathbf{I}] + \dots \\ & \quad + k(k-1)\beta \nabla J \nabla J^\top - J^2 \nabla^2 \beta) v_2 \\ &= q_2^2 (-4k\beta J^{1.5} - J^2 v_2^\top \nabla^2 \beta v_2) \end{aligned}$$

Similarly we shall have:

$$q_1 q_2 \frac{\beta^2}{J^{k-2}} v_1^\top \nabla^2 \left(\frac{J^k}{\beta} \right) |_{x_c} v_2 = q_1 q_2 (-J^2 v_1^\top \nabla^2 \beta v_2)$$

$$q_1 q_2 \frac{\beta^2}{J^{k-2}} v_2^\top \nabla^2 \left(\frac{J^k}{\beta} \right) |_{x_c} v_1 = q_1 q_2 (-J^2 v_2^\top \nabla^2 \beta v_1)$$

And since $\nabla^2 \beta$ is symmetric, $v_1^\top \nabla^2 \beta v_2 = v_2^\top \nabla^2 \beta v_1$. Now (32) can be upper bounded by:

$$\begin{aligned} & \frac{\beta^2}{J^{k-2}} q^\top \nabla^2 \left(\frac{J^k}{\beta} \right) |_{x_c} q \\ &\leq q_1^2 \left(\frac{J^2 \|\nabla\beta\|^2}{\beta} - J^2 v_1^\top \nabla^2 \beta v_1 - 4k\beta J^{1.5} \right) + \\ & \quad q_2^2 (-4k\beta J^{1.5} - J^2 v_2^\top \nabla^2 \beta v_2) + \\ & \quad q_1 q_2 (-J^2 v_1^\top \nabla^2 \beta v_2) + q_1 q_2 (-J^2 v_2^\top \nabla^2 \beta v_1) \\ &= -4k\beta J^{1.5} + q_1^2 \left(\frac{J^2 \|\nabla\beta\|^2}{\beta} - J^2 v_1^\top \nabla^2 \beta v_1 \right) + \\ & \quad q_2^2 (-J^2 v_2^\top \nabla^2 \beta v_2) + 2q_1 q_2 (-J^2 v_1^\top \nabla^2 \beta v_2) \\ &\leq -4k\beta J^{1.5} + \\ & \quad J^2 \left(\frac{\|\nabla\beta\|^2}{\beta} + |v_1^\top \nabla^2 \beta v_1| + |v_2^\top \nabla^2 \beta v_2| + |v_1^\top \nabla^2 \beta v_2| \right) \end{aligned}$$

Recall that to make the workspace valid, $\mathcal{B}_{x_t}(r_t)$ should not intersect $\partial\mathcal{F}$, then in $\mathcal{B}_{x_t}(\delta_t)$, $\beta_i > (r_t - \delta_t)^2$ for $i \in \{0 \dots m\} \Rightarrow \beta > (r_t - \delta_t)^{2m}$, and $J \leq r_t^4$. So as long as

$$\begin{aligned} k > k_2 = \\ & \frac{r_t^2}{4(r_t - \delta_t)^{2m}} \left[\sup_{x_c \in \mathcal{B}_{x_t}(\delta_t)} \left(\frac{\|\nabla\beta\|^2}{\beta} + \right. \right. \\ & \quad \left. \left. |v_1^\top \nabla^2 \beta v_1| + |v_2^\top \nabla^2 \beta v_2| + |v_1^\top \nabla^2 \beta v_2| \right) \right] \end{aligned}$$

we shall satisfy $q^\top \nabla^2 \left(\frac{J^k}{\beta} \right) |_{x_c} q < 0$ for any $q \in \mathbb{R}^n$ and any critical point x_c in $\mathcal{B}_{x_t}(\delta_t)$ other than x_t is guaranteed to be local maximum of $\frac{J^k}{\beta}$.

To sum up two cases, $k > k_0 = \max\{k_1, k_2\}$ will guarantee any critical point in $\mathcal{B}_{x_t}(\delta_t)$ to be local maximum of $\frac{J^k}{\beta}$.

□